Neurobiology of Disease 159 (2021) 105480

Contents lists available at ScienceDirect

Neurobiology of Disease

journal homepage: www.elsevier.com/locate/ynbdi

Prolonged NCX activation prevents SOD1 accumulation, reduces neuroinflammation, ameliorates motor behavior and prolongs survival in a ALS mouse model

Serenella Anzilotti [a], Valeria Valsecchi [b], Paola Brancaccio [b], Natascia Guida [a], Giusy Laudati [b], Valentina Tedeschi [b], Tiziana Petrozziello [b], Francesco Frecentese [c], Elisa Magli [c], Brenda Hassler [b], Ornella Cuomo [b], Luigi Formisano [b], Agnese Secondo [b], Lucio Annunziato [a], Giuseppe Pignataro [b,*]

[a] IRCCS SDN, Naples, Italy
[b] Division of Pharmacology, Department of Neuroscience, Reproductive and Dentistry Sciences, School of Medicine, University of Naples "Federico II", 80131 Naples, Italy
[c] Department of Pharmacy, School of Medicine, University of Naples "Federico II", 80131 Naples, Italy

ARTICLE INFO

Keywords:
ALS
Na+/Ca2+ exchanger
SOD1^{G93A} mice
Motor neurons
Neurounina
Misfolded SOD1

ABSTRACT

Imbalance in cellular ionic homeostasis is a hallmark of several neurodegenerative diseases including Amyotrophic Lateral Sclerosis (ALS). Sodium-calcium exchanger (NCX) is a membrane antiporter that, operating in a bidirectional way, couples the exchange of Ca^{2+} and Na^{+} ions in neurons and glial cells, thus controlling the intracellular homeostasis of these ions. Among the three NCX genes, *NCX1* and *NCX2* are widely expressed within the CNS, while *NCX3* is present only in skeletal muscles and at lower levels of expression in selected brain regions. ALS mice showed a reduction in the expression and activity of NCX1 and NCX2 consistent with disease progression, therefore we aimed to investigate their role in ALS pathophysiology. Notably, we demonstrated that the pharmacological activation of NCX1 and NCX2 by the prolonged treatment of SOD1^{G93A} mice with the newly synthesized compound neurounina: (1) prevented the reduction in NCX activity observed in spinal cord; (2) preserved motor neurons survival in the ventral spinal horn of SOD1^{G93A} mice; (3) prevented the spinal cord accumulation of misfolded SOD1; (4) reduced astroglia and microglia activation and spared the resident microglia cells in the spinal cord; (5) improved the lifespan and mitigated motor symptoms of ALS mice.

The present study highlights the significant role of NCX1 and NCX2 in the pathophysiology of this neurodegenerative disorder and paves the way for the design of a new pharmacological approach for ALS.

1. Introduction

Amyotrophic lateral sclerosis is an idiopathic, fatal neurodegenerative disease of the human motor system. The clinical hallmark is the selective motor neurons (MNs) death in the brain and spinal cord, leading to the paralysis of voluntary muscle (Pasinelli and Brown, 2006).

ALS is relentlessly progressive, 50% of patients die within 30 months of symptoms onset (Hand et al., 2002). Only 5–10% of ALS cases are familial (FALS), the remaining are sporadic, i.e., occurring in individuals with no family history of ALS. The best documented familiar form of ALS is due to inherited mutations in SOD1, the gene encoding copper–zinc superoxide dismutase (Rosen et al., 1993).

Currently, the NMDA blocker riluzole and the ROS scavenger edaravone represent the only two therapeutic options available (Jaiswal, 2019). Riluzole acts by increasing the survival of patients by 2–3 months; edaravone, acts to slow disease progression as measured by ALSFRS-R to evaluate motor function of patients (Jaiswal, 2019).

Among the different pathophysiological mechanisms proposed for ALS neurodegeneration, the selective vulnerability of MNs has been linked to the inability of these cells to control the dysregulation of sodium and calcium homeostasis (Berridge et al., 2003; Grosskreutz et al., 2010; Guerini et al., 2005). Sodium-calcium exchanger (NCX) is a membrane antiporter strongly involved in the maintenance of Ca^{2+} and Na^{+} homeostasis. Indeed, operating in a bidirectional way, it couples the

* Corresponding author.
E-mail address: giuseppe.pignataro@unina.it (G. Pignataro).

https://doi.org/10.1016/j.nbd.2021.105480
Received 8 April 2021; Received in revised form 9 July 2021; Accepted 9 August 2021
Available online 16 August 2021

exchange of Ca^{2+} and Na^{+} ions in neurons and glial cells (Blaustein and Lederer, 1999; Cuomo et al., 2015). Among the three NCX genes, *NCX1* and *NCX2* are widely expressed within the CNS, while *NCX3* is present only in skeletal muscles and at lower levels of expression in selected brain regions (Canitano et al., 2002; Papa et al., 2003; Quednau et al., 1997).

In the light of these premises, we investigated the involvement of NCX1 and NCX2 in the pathogenesis of ALS and their possible "druggability". To achieve this aim, we used the newly synthesized compound neurounina, a diazepine derivative, able to activate NCX1 and NCX2, with no effect on NCX3, and provided with an estimated EC_{50} in the low nanomolar ranges (Molinaro et al., 2013). Relevantly, preclinical studies showed that neurounina is provided with a high lipophilicity index, low toxicity and ability to cross the BBB when systemically administered (Severino et al., 2019).

In order to deeply investigate the role of these two NCX isoforms, NCX1 and NCX2, prominently expressed within the CNS, in a familial model of ALS it will be assessed: (1) mRNA and protein expression of NCX1 and NCX2 in spinal cord of $SOD1^{G93A}$ mice; (2) whether misfolded SOD1 aggregation observed in SOD^{G93A} mice is linked to changes in NCX1 and NCX2 activity; (3) whether the modification of NCX1 and NCX2 expression and activity in ALS mice is accompanied by changes in microglia and astroglia function; and (4) whether the pharmacological activation of NCX1 and NCX2 activity might interfere with ALS symptomatology and survival rate.

2. Materials and methods

2.1. Animal model

B6SJL-TgN SOD1/G93A(+)1Gur mice expressing high copy number of mutant human SOD1 with a Gly93Ala substitution [$SOD1^{G93A}$] and B6SJL-TgN (SOD1)2Gur mice expressing wild-type human SOD1 (WT) were obtained from Jackson Laboratories (Bar Harbor, ME, USA). This model was used for experiments as it remains the only validated mouse model of ALS for preclinical study according to the ALS Therapy Development Institute and reproduces much of the pathogenesis and pathology of clinical disease.

Transgenic animals have been crossed with background-matched B6SJL wild-type female and selective breeding maintained each transgene in the homozygous state. All transgenic mice were identified analyzing extracts from tail tips by staining for SOD1 as previously described (Anzilotti et al., 2018).

Overall, 130 male and female mice were group housed in microisolator caging under standard 12-h light–dark conditions with access to food and water. 7 males and 5 females out of 120 animals were not included in the experimental groups as they died for unknown reasons. The number of female and male mice was balanced among all the experimental groups. Dead animals were equally distributed among the experimental groups. Experiments were performed according to the international guidelines for animal research and approved by the Animal Care Committee of "Federico II" University of Naples, Italy and Ministry of Health, Italy. All efforts were made to minimize animal suffering and to reduce the number of animals used.

2.2. Neurounina treatment

The NCX1, NCX2 activator neurounina, 7-nitro-5-phenyl-1-(pyrrolidin-1-ylmethyl)-1Hbenzo[e][1,4]diazepin-2(3H)-one, was synthesized as previously described (Molinaro et al., 2013), dissolved in distilled water and intraperitoneally (IP) administered daily at a dose of 30 μg/kg. This dosage was chosen from considerations deriving from the chronic use of 30 μg/kg neurounina, daily for 3 weeks, in a model of neonatal hypoxia (Cerullo et al., 2018) and from pharmacokinetic considerations (neurounina half-life 2.5 h) (Severino et al., 2019). At postnatal day 60 (P60), $SOD1^{G93A}$ mice were randomized to receive either neurounina or vehicle control by IP every day for 60 days.

2.3. Tissue processing, immunostaining, and confocal immunofluorescence

Immunostaining and confocal immunofluorescence procedures were performed as previously described (Gargiulo et al., 2016; Pignataro et al., 2015). Animals were anesthetized and transcardially perfused with saline solution containing 0.01 ml heparin, (10 U/ml heparin in 0.1 M PBS) followed by 60 ml of 4% paraformaldehyde.

Spinal cords were rapidly removed on ice and postfixed overnight at +4 °C and cryoprotected in 30% sucrose in 0.1 M phosphate buffer (PB) with sodium azide 0.02% for 24 h at 4 °C. Spinal cords were then sectioned frozen on a sliding cryostat at 40 μm thickness, in rostrum-caudal direction. Afterwards, free floating serial sections were incubated with PB Triton X 0.3% and blocking solution (0.5% milk, 10% FBS, 1% BSA) for 1 h and 30 min. The sections were incubated overnight at +4 °C with the following primary antibodies: anti-SMI32(mouse monoclonal antibody; 1:1000; Biolegend, San Diego, CA, catalog 801,701), anti-NCX1 (mouse monoclonal; 1:500; Swant, Switzerland, catalog 11–13); anti-NCX2 (1:500; Alpha Diagnostic San Antonio, TX, catalog ncx21-A); anti-NCX3 (rabbit polyclonal 1:4000; Swant, Switzerland, catalog 95,209), anti-Glial Fibrillary Acidic protein (GFAP, rabbit polyclonal antibody; 1:500; Abcam, Cambridge, UK, catalog AB7260) and anti-ionized calcium binding adaptor molecule 1 (Iba1, rabbit polyclonal antibody; 1:500; Wako Diagnostic USA, catalog 019–19,741) anti-TMEM119 (mouse monoclonal 1:500; Synaptic Systems; Germany, catalog 400,011), anti-Choline Acetyltransferase (CHAT, rabbit polyclonal antibody; 1:300; Millipore, Milan, Italy, catalog AB143).

The sections were then incubated with the corresponding florescent-labeled secondary antibodies, Alexa 488/Alexa 594 conjugated anti-mouse/antirabbit IgGs (Jackson ImmunoResearch Baltimore, PA). Nuclei were counterstained with Hoechst (Sigma-Aldrich, Milan, Italy). Images were observed using a Zeiss LSM700 META/laser scanning confocal microscope (Zeiss, Oberkochen, Germany). Single images were taken with an optical thickness of 0.7 μm and a resolution of 1024 × 1024. In double-labeled sections, the pattern of immune reactivity for both antigens was identical to that seen in single-stained material. Control double-immunofluorescence staining entailed the replacement of the primary antisera with normal serum (data not shown). To minimize a possible cross-reactivity between IgGs in double immunolabeling experiments, the full complement of secondary antibodies was maintained but the primary antisera were replaced with normal serum or only one primary antibody was applied (data not shown). In addition, the secondary antibodies were highly preadsorbed to the IgGs of numerous species (Cantarella et al., 2014). Tissue labeling without primary antibodies was also tested to exclude autofluorescence. No specific staining was observed under these control conditions, thus confirming the specificity of the immunosignals.

Nissl staining was performed as previously described (Cerullo et al., 2018). Briefly, slide-mounted sections were dipped 7 min in 0.5% solution of Cresyl Violet in distilled water supplemented with acetic acid (16 N solution, 60 drops/l). Slides were then rinsed in distilled water, dehydrated through graded ethanol baths (95%, 100%; 5 min each), delipidated 8 min in xylene, and coverslipped with Eukitt Mounting Medium (Bio-Optica, Milan, Italy).

Standard 3,3′-diaminobenzidine (DAB) staining was employed on sagittal step serial sections using antibody directed against B8H10 (Leyton-Jaimes et al., 2016) (mouse monoclonal 1:500 MEDIMABS, Montreal (Quebec) Canada, catalog MM-0070-P).

2.4. Fluorescence intensity analysis

Quantification of GFAP, Iba1 and TMEM119 fluorescence intensity on tissue sections at the level of the lumbar spinal cord (L1-L6), was

quantified in terms of pixel intensity value by using the NIH image software, as previously described (Anzilotti et al., 2018). Briefly, digital images were taken with ×20 or ×10 objective and identical laser power settings and exposure times were applied to all the photographs from each experimental set. Images were first thresholded to identify the positive signal; subsequently, the pixels expressing GFAP, Iba1 and TMEM119 were identified. Finally, the number of pixels positive for GFAP, Iba1 and TMEM119 was measured per microscope field. Images from the same areas of each brain region were compared. Results were expressed in arbitrary units. $n = 3$ mice per treatment group and six sections for each genotype.

2.5. Motor neurons and Misfolded-SOD1 counting analysis

MNs were counted in the spinal cord. Sections of each area were analyzed as previously described (Valsecchi et al., 2020). Frozen brain tissue and spinal cord were sectioned on a sliding cryostat at 20 μm, in rostrum-caudal direction. Analyses were performed using image J software in Polygonal-shaped neurons larger than 200 μm^2 with a well-defined cytoplasm, nucleus, and nucleolus for MNs counting. Quantification of MNs was determined by counting and averaging 4 sections selected at equally spaced intervals spanning L1–6 under 20× magnification, $n = 6$ mice for each genotype were analyzed. Cell counting analysis was determined as total MNs per field (mm^2) of 4.5 month-old mice. For Mis-SOD1 counting the total number of positive signals of B8H10 antibody (Leyton-Jaimes et al., 2016) was counted by image J software, for photographic field (mm^2) in cells with well-defined cytoplasm. $n = 3$ mice per treatment group and six sections for each genotype.

2.6. Iba1, GFAP and TMEM119 cell counting analysis

Frozen spinal cord was sectioned on a sliding cryostat at 20 μm, in rostrum-caudal direction. Images from the same areas of each brain region were compared. Analyses were performed using image J software in the total number of positive signals of Iba1, GFAP and TMEM119 antibodies for photographic field (mm2) in lumbar spinal cord (L1-L6) of Wt and G93A mice. $n = 3$ mice per treatment group and six sections for each genotype (Coda et al., 2021).

2.7. Western blot analysis

For western blot analysis, spinal cord tissues were lysed in lysis buffer containing 50 mM Tris–HCl, pH 7.4, 150 mM NaCl, 1 mM EDTA, 1% Triton X-100, and protease and phosphatase inhibitors. Samples were subjected to SDS-polyacrylamide gel electrophoresis (SDS-PAGE) and immunoblotted with specific antibodies. Rabbit polyclonal antibody against NCX1 (1:1000 dilution, Swant, Bellinzona, Switzerland), rabbit polyclonal anti-NCX2 (1:500 dilution, ALPHA-DIAGNOSTIC int. San Antonio, TX, USA), and mouse monoclonal anti- β-Actin-peroxidase, (1:10000 dilution, Sigma-Aldrich, St. Louis, MO, USA. Immunoreactive bands were detected using ECL (GE Healthcare, Milan, Italy). The optical density of the bands (normalized for β-actin) was determined by Chemi-Doc Imaging System (Bio-Rad, Segrate, Italy). The optical density of NCX1 was determined for the band at 120 KDa.

2.8. RT-PCR experiments

Tissues were quickly removed from mice, then immediately frozen on dry ice and stored at −80 °C until use. Total RNA was extracted with Trizol reagents, following supplier's instructions (Life Technologies, Monza, Italy). The first-strand cDNA was synthesized with 2 μg of total RNA using the High Capacity cDNA Reverse Transcription Kit following supplier's instruction (Life Technologies). Quantitative real-time PCR with TaqMan assays for NCX1-2-3 genes and glucuronidase beta (Gusb) as housekeeping were performed in a 7500 real-time PCR system (Life Technologies). Samples were amplified simultaneously in triplicate in 1 assay run. Changes in mRNA levels were determined as the difference in threshold cycle (−Δ Ct) between the target gene and the reference gene (Valsecchi et al., 2020; Valsecchi et al., 2015).

2.9. Cell lines

Human neuroblastoma SH-SY5Y cells (Cell bank Line Collection ICLC) were grown as monolayers in Dulbecco's modified Eagle's medium (DMEM) with 10% (v/v) fetal bovine serum (FBS), L glutamine (2 mM), pyruvic acid (1 mM), 1× non-essential amino acids and 1× antibiotics.

2.10. Purified synaptosomal preparation and $[Ca^{2+}]_i$ imaging

Spinal cord synaptosomes were purified on discontinuous Percoll gradients, as previously described(Secondo et al., 2015). Briefly, tissues were homogenized in a medium containing 0.32 M sucrose, 1 mM EDTA, and 0.25 mM dl-dithiothreitol (pH 7.4). Each homogenate was centrifuged at 1000 ×*g* for 10 min at 4 °C and the supernatant was diluted at 14 ml/g with sucrose medium (pH 7.4). Two ml of the suspension were placed onto 8 ml Percoll discontinuous gradient containing 0.32 M sucrose and 3%, 10%, 15%, and 23% Percoll (pH 7.4). After centrifugation at 32,000 ×*g* for 15 min at 4 °C, synaptosomes were recovered between the 15% and 23% Percoll bands, diluted five times with HEPES buffer medium containing (in mM): 125 NaCl, 2.5 KCl, 5 $NaHCO_3$, 1.2 NaH_2PO_4, 1.2 $MgSO_4$, 6 glucose, and 25 HEPES (pH 7.4), and centrifuged at 15,000 ×*g* for 15 min at 4 °C. Finally, the pellet was resuspended in 1 ml of medium B (145 mM NaCl, 3 mM KCl, 1.2 mM $MgCl_2$, 10 mM glucose, and 10 mM HEPES, pH 7.4) and stored on ice. Protein content was determined by the Bradford method. Percoll-purified synaptosomes were resuspended in medium B (1 mg/ml) and loaded with the ratiometric fluorescent Ca^{2+} indicator Fura-2 AM (6 μM) in the presence of 16 μM bovine serum albumin for 45 min at 37 °C. Dye-loaded synaptosomes were then washed by centrifugation, re-suspended in medium B containing 1.2 mM $CaCl_2$, and attached to poly-D-lysine-coated coverslips for 20 min at 37 °C. The coverslips were placed into a perfusion chamber (Medical System, Greenvale, NY, USA) mounted on the stage of an inverted Zeiss Axiovert 200 fluorescence microscope (Zeiss, Oberkochen, Germany) equipped with a × 40 oil objective lens. Experiments were carried out with a digital imaging system composed of MicroMax 512BFT cooled CCD camera (Princeton Instruments, Trenton, NJ, USA), LAMBDA 10–2 filter wheel (Sutter Instruments, Novato, CA, USA), and META-MORPH/METAFLUOR Imaging System software (Universal Imaging, West Chester, PA, USA). Synaptosomes were illuminated at 340 and 380 nm wavelength by a 100-W Xenon lamp (Osram, Berlin, Germany). The emitted light was passed through a 512 nm barrier filter. Images were digitized and analyzed using metafluor Imaging software. $[Ca^{2+}]_i$ in SH-SY5Y cells was detected by single-cell Fura-2/AM computer assisted video-imaging, as previously reported (Formisano et al., 2013). Cells were loaded in normal Krebs solution containing (in mM) 5.5 KCl, 160 NaCl, 1.2 MgCl2, 1.5 CaCl2, 10 glucose and 10 Hepes–NaOH, pH 7.4. Intracellular Ca^{2+} concentration was calculated by the equation of Grynkiewicz et al. (Grynkiewicz et al., 1985; Urbanczyk et al., 2006).

NCX activity was evaluated as Ca^{2+} uptake through the reverse mode by switching the normal Krebs medium to Na^+-deficient $NMDG^+$ medium named Na^+-free, containing (in mM): 5.5 KCl, 147 NMDG, 1.2 $MgCl_2$, 1.5 $CaCl_2$, 10 glucose, and 10 Hepes-Trizma (pH 7.4). These experiments with SH-SY5Y cells were performed in the presence of the irreversible and selective inhibitor of the sarco(endo)plasmic reticulum Ca^{2+} ATPase thapsigargin (1 μM).

2.11. Cell transfection of plasmids and small interfering RNAs

After 24 h of cell seeding, cells were transiently transfected with 10

μg -for Immunoprecipitation experiments- or 1 μg -for MTT assay- of plasmids containing SOD1 wild type (SOD1-WT) cDNA or SOD1 cDNA carrying the mutation G93A (SOD1-G93A), that were a gift from Elizabeth Fisher (Addgene plasmid # 26397 and # 26401), by using Lipofectamine 2000 in Optimem medium, according to the protocol by the manufacturer (Invitrogen, ThermoFisher Scientific). The next day, cells have been treated with Neurounina-1 (30 nM) or vehicle and, after 24 h, have been analyzed for immunoprecipitation experiments or MTT assay.

NCX1 and NCX2 knocking-down was achieved by different FlexiTube small interfering RNAs (siRNAs) against the proteins (Qiagen, Milan, Italy). Cells were transfected in OptiMem medium by HiPerFect Transfection Reagent with the non-targeting control or the following siRNAs in combination (each at 10 nM):

(1) Hs_SLC8A1_9 (target sequence: CAGGCCATCTTCTAAGACTGA);
(2) Hs_SLC8A1_8 (target sequence:ATGCGGCGATTAAGTCTTTCA);
(3) Hs_SLC8A1_7 (target sequence: GAGGTGGTGATTTGACTAACA);
(4) Hs_SLC8A1_6 (target sequence: CTGATCGGTTCATGTCCTCTA);
(5) Hs_SLC8A2_10 (target sequence: CGAGGGCACGCTGGTGTTCAA);
(6) Hs_SLC8A2_9 (target sequence: CCCGAAGAGCATCGAGCTGGA);
(7) Hs_SLC8A2_8 (target sequence: CTGTTGATGTTTCCTGCCCAA);
(8) Hs_SLC8A2_7 (target sequence: CCCTGACACGTTCGCCAGCAA).

2.12. Immunoprecipitation

For immunoprecipitation total cell extracts for each group were resuspended using immunoprecipitation lysis buffer (50 mM Tris–HCL, pH 7.5, Triton 1%, β-glicerol 10 mM, NaF 100 mM, Na3VO4 100 mM, 150 mM NaCl, and 1 mM EDTA), with the addition of protease inhibitor cocktail (1/100) P-8140 (Sigma). Aliquots of 1500 μg were used for the experiments in a final volume of 500 μl and 3 μg of mouse monoclonal anti-misfolded SOD1 (B8H10, MEDIMABS) (Leyton-Jaimes et al., 2016) was added to each treatment set; the samples were then placed on a rocker at 4 °C overnight. Notably, 100 μg of pre-immunoprecipitated sample was used as input. After a centrifugation at 2500 rpm for 5 min, the supernatant was discarded, and the pellets were washed two times with 1 ml of cold PBS 1× plus protease inhibitors. The pellet was re-suspended in 20 μl of loading buffer 2×, boiled for 10 min and centrifuged (Guida et al., 2017). The immunoprecipitated supernatant was separated by SDS-12% and blotted onto polyvinylidene difluoride membrane (Amersham Biosciences). Membranes were then treated with a blocking solution for 2 h at RT and incubated overnight at 4° with rabbit-polyclonal anti-SOD1 (1:1000, PA5–27240,ThermoFisher Scientific) (Laudati et al., 2019).

2.13. L-BMAA exposure

After plating, SH-SY5Y cells were exposed to the cyanobacterial toxin β-*N*-methylamino-L-alanine (L-BMAA) at 2 mM for 120 h in a medium containing 0% FBS. The neurotoxin was replaced at day 1, 3 and 5 while neurounina (10 nM) was added to the cell culture medium 20 min before each L-BMAA administration. At the end of the experiment, cell viability was assessed by MTT assay.

2.14. Determination of cell viability

Cell viability was revealed as previously described (Amoroso et al., 2000; Laudati et al., 2019) by using the MTT (Sigma- Aldrich, Milan Italy).

Specifically, after 24 h of treatment with neurounina 30 nM or vehicle, the medium was removed, and cells were incubated in 0.5 mg/ml of MTT solution for 2 h at 37 °C. The incubation was stopped by adding 500 μl of acidified isopropanol to solubilize the formazan salt, and viability was read by measuring the absorbance at 540 nm with a spectrophotometer.

2.15. Evaluation of motor performance

Hind limb grip test was conducted by placing the mouse on a grid (45 cm long × 28 cm large) upside-down (30 cm above a foam pad). The test was performed once a week and the latency to fall off the grid was also measured up to a maximum of 60 s.(Anzilotti et al., 2015). Paralysis onset was defined as the day in which the grip test performance was less than 20% compared to day 1 performance.

Motor coordination and balance was assessed using a five-station mouse rotarod apparatus (Ugo Basile; Milan, Italy) as previously described (Natale et al., 2020). In each station, the rod was 6 cm in length and 3 cm in diameter. Mice were trained to maintain balance at increasing speed up to a constant speed of 14 rpm for three consecutive trials. The test sessions were conducted by one rotarod trial administered once a week. In this session, the speed of rotation was increased from 4 to 14 rpm over 60 s. Mice had three trials on the rod, and the latencies to fall were measured once a week and then averaged. The maximum latency of 60 s was assigned to the mice that did not fall at all. Weekly evaluation of hind limb paralysis was performed. Hind limb paralysis was scored when the animal dragged one of its hind limbs, and paralysis of a forelimb was scored when the mouse failed to use its forelimbs for walking or righting. Body weight was measured immediately before each session of behavioral tests.

Disease end stage was defined by the inability of mice to right themselves within 20 s when placed on their sides. We did not identify any differences between males and females for this reason we decided to use both genders.

For the evaluation of survival and motor performance we considered two different experimental groups:

Group 1-Survival: $n = 10$ (5 males and 5 females) G93A mice treated with vehicle and $n = 12$ (6 males and 6 females) G93A mice treated with neurounina.

Group 2-Onset disease and motor performance: $n = 16$(7 males and 9 females) G93A mice treated with vehicle; $n = 15$ (7 males and 8 females) G93A mice treated with neurounina; $n = 6$ (3 males and 3 females) Wild type mice treated with vehicle and n = 6 (3 males and 3 females) Wild type mice treated with neurounina.

2.16. Statistical analysis

Data were evaluated as means ± SEM. Statistically significant differences among means were determined by one-way ANOVA followed by Student–Newman–Keuls/Bonferroni post-hoc test for western blotting, cell counting, real-time PCR analysis, microfluorimetry and Behavioral test. The Kaplan–Meier plot was used to evaluate survival, grip, rotarod and paralysis onset. Student's *t*-test was used for two groups comparison. Statistical significance was accepted at the 95% confidence level ($p < 0.05$). Statistical analyses were performed by using GraphPad Prism 5.0 (La Jolla, CA, USA). All experiments were carried out in a blinded manner.

3. Results

3.1. NCX1 transcript and protein expression was downregulated in spinal cord of fully symptomatic $SOD1^{G93A}$ mice, whereas NCX2 transcript expression decreased both in presymptomatic and fully symptomatic $SOD1^{G93A}$ mice

To examine the role of NCX1 and NCX2 in ALS, transcript and protein levels were evaluated in the spinal cord of asymptomatic (2 months) and late (4.5 months) symptomatic $SOD1^{G93A}$ mice. These values of transcripts and proteins were compared to those of age-matched healthy controls (Wt) (Fig. 1).

At 2 months of age, when $SOD1^{G93A}$ mice were still asymptomatic, no significant difference in NCX1 mRNA and protein expression levels were found in the spinal cord of $SOD1^{G93A}$ compared to Wt littermate

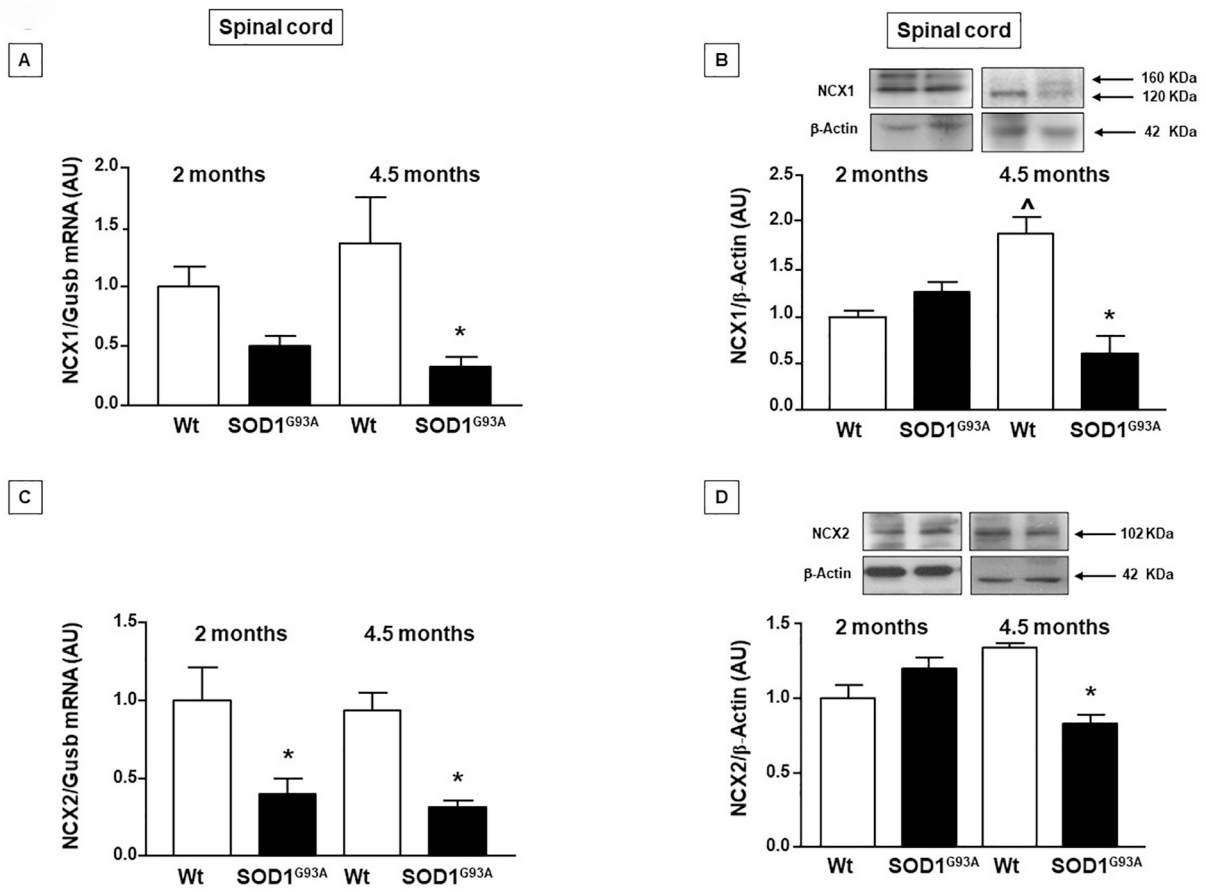

Fig. 1. Evaluation of NCX1and NCX2 transcripts and protein expressions in spinal cord tissues from SOD1^{G93A}mice compared to age-matched healthy controls (Wt). (A) and (B) show mRNA levels and protein of NCX1 at 2 months and 4.5 months of age in spinal cord of Wt and SOD1^{G93A}mice. mRNA expression levels were normalized for beta-glucuronidase (GUSB). Protein expression levels were normalized with β-actin. (C) and (D) show mRNA and proteins levels of NCX2 at 2 months and 4.5 months of age in spinal cord of Wt and SOD1^{G93A}mice. Real time PCR, data are expressed as mean ± SEM ($n = 3/6$ for each group). Western blotting analysis, data are expressed as mean ± SEM (n = 3/5 for each group). Statistically significant differences among means were determined by one-way ANOVA followed by Newman Keuls's correction for multiple comparisons test: * $p < 0.05$, SOD1^{G93A} vs. Wt; ^ $p < 0.05$, Wt 4.5 months vs. Wt 2 months.

(Fig. 1A–B). By contrast, at 4.5 months of age, when SOD1^{G93A} mice were fully symptomatic, NCX1 mRNA ad protein levels in the spinal cord significantly decreased by 70% compared to Wt animals (Fig. 1A–B). In contrast, NCX2 mRNA expression was down-regulated in the spinal cord in the pre-symptomatic phase and in the late phase of the disease (approximately 70% reduction) (Fig. 1C). In a similar manner, also NCX2 protein expression showed a significant decrease in the late phase of the disease (Fig. 1D).

3.2. *The NCX1 and NCX2 activator, neurounina, prevented the reduced NCX activity observed in spinal cord of SOD1^{G93A} mice*

In order to prevent NCX1 and NCX2 reduced activity observed in the spinal cord of SOD1^{G93A} mice, the newly synthesized NCX1 and NCX2 activator, neurounina, was intraperitoneally administered daily at a dose of 30 μg/kg, (Molinaro et al., 2013) beginning at 2 months of age until 4.5 months. The effect of neurounina on NCX1 and NCX2 activity and expression was evaluated by microfluorimetry, immunohistochemical, and western blotting analyses, respectively (Fig. 2). In particular, NCX reverse mode of operation was evaluated by Na^+-free-induced $[Ca^{2+}]_i$ increase in spinal cord synaptosomes obtained from Wt and SOD1^{G93A} mice treated with vehicle or with neurounina, at 4.5 months of age. Na^+-free-induced $[Ca^{2+}]_i$ increase was significantly reduced in spinal cord synaptosomes from vehicle-treated SOD1^{G93A} mice compared to vehicle-treated Wt animals (Fig. 2A). Interestingly, long-lasting neurounina treatment in vivo was able to increase the activity of NCX in Wt mice and to prevent the reduction of NCX activity observed in spinal cord synaptosomes from symptomatic SOD1^{G93A} mice (Fig. 2A) without interfering with NCX expression. In fact, western blotting analysis showed that neurounina treatment did not alter NCX1, NCX2 (Fig. 2B) and NCX3 (data not shown) expression in the spinal cord of Wt and symptomatic SOD1^{G93A} mice. In agreement with these data, confocal microscopy experiments with antibodies directed against a specific MNs marker, SMI32, and against NCX1 and NCX2, indicated that NCX1 and NCX2 expression decreased in spinal cord motor neurons of symptomatic SOD1^{G93A} mice (Fig. 2Ca-d,i-l;Da-d,i-l). Furthermore, the neurounina treatment did not induce any change in the expression and the localization of NCX1 (Fig. 2Ce-h,m-p) and NCX2 (Fig. 2De-h,m-p). Interestingly, the expression of NCX1 and NCX2 was prevalent in the cytosol of large polygonal-shaped MNs (Fig. 2Ca-d;Da-d).

3.3. *Neurounina treatment prolonged motor neurons survival in the ventral spinal horn of SOD1^{G93A} mice*

In order to investigate whether NCX1 and NCX2 increased activity, induced by neurounina, had a neuroprotective effect on MNs, spinal cord sections from fully symptomatic mice were stained with Nissl, and MNs number was evaluated in the ventral spinal cord region. Since in ALS pathophysiology the degeneration occurs preferentially in large MNs, the number of cells with a perikaryal projection area of more than 200 μm^2 was counted in Wt and fully symptomatic SOD1^{G93A} mice treated chronically with vehicle or with neurounina (Fig. 3A). The

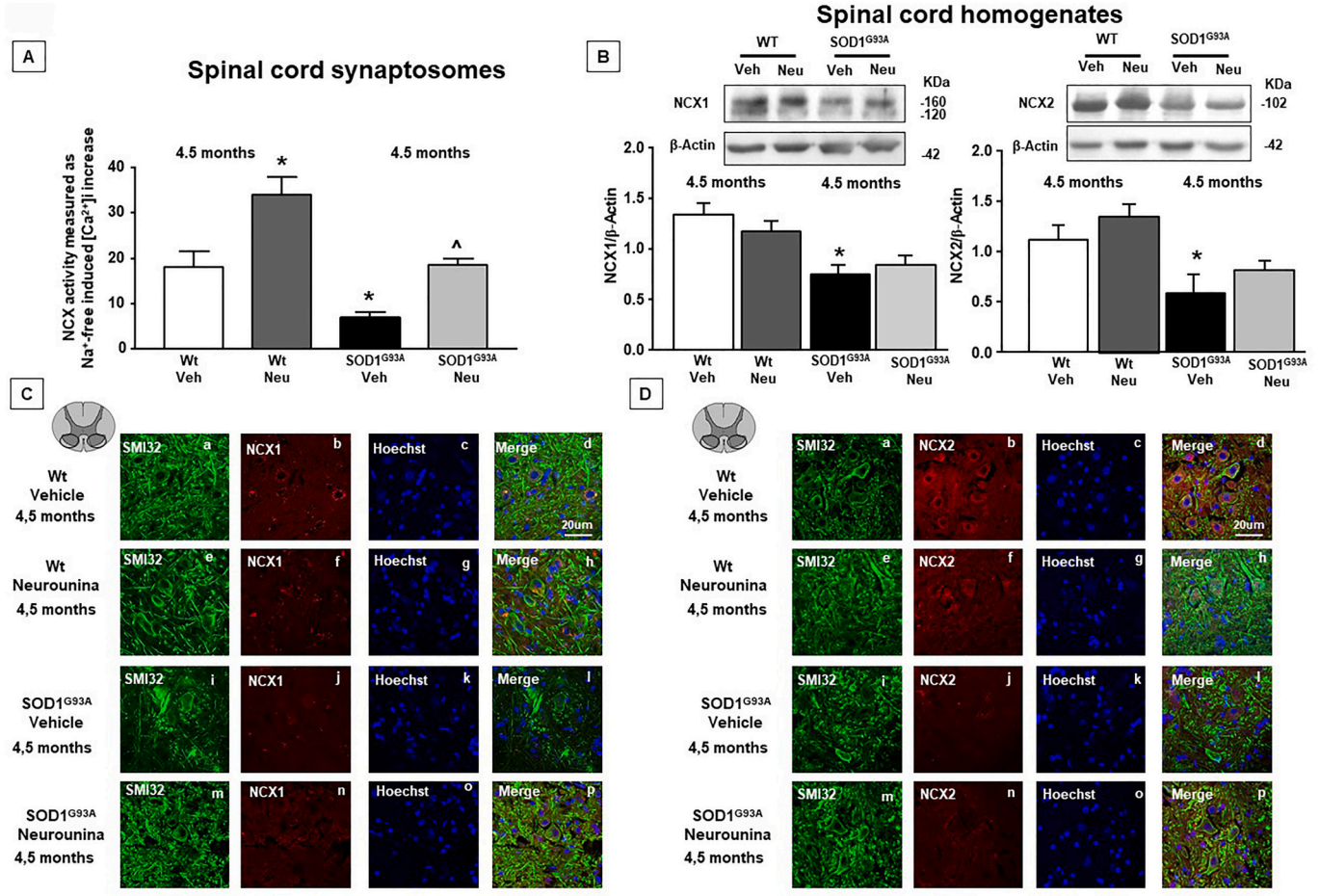

Fig. 2. NCX1 and 2 immunolocalization, expression and quantification of NCX activity in SOD1^{G93A} mice treated to neurounina.
(A) Quantification of NCX activity as [Ca^{2+}]i increase induced by Na^{+} −free perfusion in Fura-2 AM-loaded spinal cord synaptosomes of adult wild-type (Wt) mice treated with vehicle, Wt mice treated with neurounina and symptomatic SOD1^{G93A} mice treated with vehicle or neurounina. *P* values were obtained using one-way ANOVA with Newman Keuls's correction for multiple comparisons. *$P < 0.05$ vs. wild-type vehicle and wild-type neurounina; ^$P < 0.05$ vs. SOD1^{G93A} mice vehicle; (B) Representative western blotting and quantification of the effect of neurounina on NCX1–2 protein expression, arbitrary units (AU), in spinal cord. Statistically significant differences among means were determined by one-way ANOVA followed by Newman Keuls's correction for multiple comparisons. The β-actin expression level was used for normalization. Data are expressed as mean ± SEM ($n = 4/5$ for each group). * $p < 0.05$, Wt vs SOD1^{G93A} mice.
Double labeling of NCX1 and NCX2 with SMI-32 in spinal cord of Wt mice + vehicle (C a-d, D a-d), Wt mice + neurounina (C e-h, D e-h) SOD1^{G93A} mice + vehicle (C i-l, D i-l) SOD1^{G93A} mice + neurounina (C m-p, Dm-p) Scale bar 20 μm.

results revealed that neurounina treatment preserved large MNs in the spinal cord of fully symptomatic SOD1^{G93A} mice (Fig. 3B). The neuroprotective effect of neurounina on MNs survival was confirmed by using Chat antibody, a specific marker of MNs. (Fig.S1). Indeed, the total number of Chat positive cells increased in neurounina G93A mice group compared to vehicle group.

3.4. Neurounina prevented the accumulation of misfolded SOD1 and enhanced the survival of neuronal cells transfected with SOD1^{G93A}

To study the involvement of NCX1 and NCX2 isoforms in the neuroprotective mechanism of neurounina, both the exchanger isoforms were efficiently silenced in human SH-SY5Y neuroblastoma cells without interfering with NCX3 expression (Fig. 4A). Under these conditions, Na^{+}-dependent NCX activity was significantly reduced compared with siControl-transfected cells (Fig. 4B). Exposure to L-BMAA toxin, causing Guamanian amyotrophic lateral sclerosis/parkinsonism dementia complex (ALS/PDC), induced cell death in SH-SY5Y that was partially prevented by neurounina treatment (Fig. 4C). Interestingly, the neuroprotective effect of neurounina was counteracted by NCX1 and NCX2 knocking down, a condition basically worsening cell survival (Fig. 4C).

To test whether NCX1 and NCX2 activation can prevent the accumulation of misfolded SOD1 (misSOD1) and protect against its toxicity, human SH-SY5Y neuroblastoma cells were transfected with WT (SOD1^{WT}) or mutant (SOD1^{G93A}) SOD1 and exposed to neurounina. The accumulation of misSOD1 was detected by immunoprecipitation (IP) with B8H10, a monoclonal antibody that recognizes misfolded forms of mutant human SOD1 protein, (Leyton-Jaimes et al., 2016) (Fig. 5A). Interestingly, neurounina treatment clearly reduced the aggregation of misfolded SOD1 in cell expressing SOD1^{G93A}, compared with vehicle-treated SOD1^{G93A} cells (Fig. 5A).

Cell survival was quantified by the MTT assay in: (1) untransfected cells, (2) SOD1^{G93A} transfected cells and (3) SOD1^{WT} transfected cells, exposed to vehicle or to neurounina (Fig. 5B). Notably, in these neuronal cells neurounina treatment was able to rescue the toxic effect induced by the SOD1^{G93A} variant transfection (Fig. 5B).

Furthermore, immunostaining of B8H10 antibody revealed that neurounina treatment significantly reduced misSOD1 in SOD1^{G93A} mice in the lumbar spinal cord area (Fig. 5C a-d). As expected, in Wt mice the B8H10 immunosignal was very low (Fig. 5C a,b). Moreover, the total number of misSOD1 positive cells significantly decreased by 60% in lumbar spinal cord of SOD1^{G93A} mice treated with neurounina (Fig. 5D).

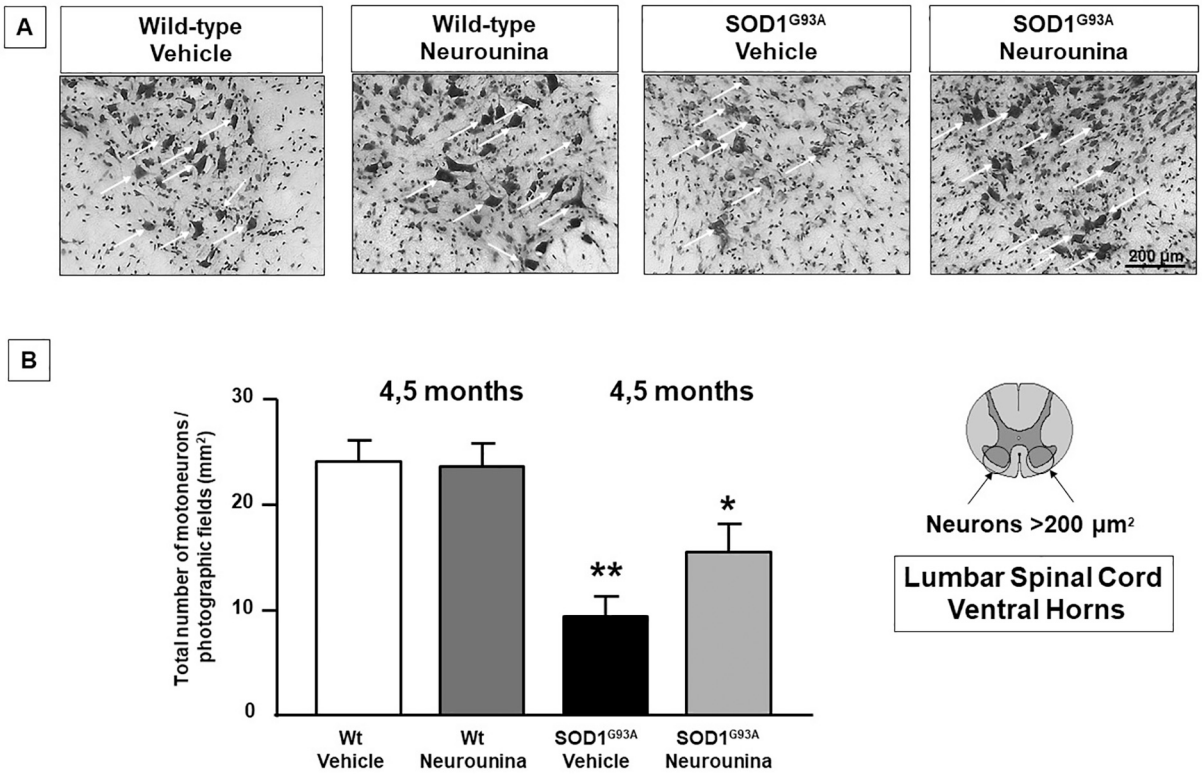

Fig. 3. Effect of neurounina on MNs survival. (A) Representative image of Nissl stained in spinal cord. Scale bar 200 µm. (B) Cell counting analysis of motor neurons are expressed as total number of motor neurons in spinal cord of 4.5 month-old SOD1^{G93A} mice treated with vehicle or neurounina compared to wild-type vehicle (Wt) and neurounina. * $p < 0.05$, ** $p < 0.01$ WT vs SOD1^{G93A} mice. Data are expressed as mean ± SEM ($n = 6$ for each group). P values were obtained using one-way ANOVA with Newman Keuls's correction for multiple comparisons.

3.5. Prolonged neurounina treatment reduced astroglia and microglia activation in the spinal cord of SOD1^{G93A} mice

In order to investigate the effect of neurounina treatment on astrogliosis and microgliosis, GFAP, Iba1 and TMEM119 immunostaining was evaluated in the spinal cord of wild-type and SOD1^{G93A} mice treated with neurounina. Scattered astrocytes cells were visualized by GFAP immunostaining in wild-type mice (Fig. 6A a,e,i), Neurounina treatment did not alter the expression of GFAP in Wt mice (Fig. 6A b,f,j). By contrast, an intense astroglia reaction was evident in the vehicle treated SOD1^{G93A} group (Fig. 6A c,g,k), these astroglia reactions were attenuated in neurounina treated SOD1^{G93A} group (Fig. 6A d,h,l). Indeed, the total number of activated GFAP cells was significantly reduced in SOD1^{G93A} neurounina treated mice compared to vehicle group. In a similar manner, also the fluorescence intensity of GFAP labeling was attenuated in SOD1^{G93A} chronic neurounina treated mice (Fig. 6B). As concern the microgliosis, a strong activation of Iba1 immunostaining was evident in SOD1^{G93A} vehicle treated mice (Fig. 6C c,g,k). This activation was reduced in neurounina treated mice (Fig. 6C d,h,l). In fact, the total number of Iba-1 activated cells and the fluorescence intensity of Iba-1 labelling were significantly reduced in SOD1^{G93A} chronic neurounina-treated mice compared to vehicle treated mice (Fig. 6D). Furthermore, in order to discriminate resident microglia from blood-derived macrophages, the expression of TMEM119 was also evaluated in all groups (Fig. 6E a-d). The number of TMEM119 positive cells as well as the its fluorescence intensity decreased in SOD1^{G93A} vehicle mice whereas in SOD1^{G93A} neurounina mice was increased (Fig. 6F).

3.6. Prolonged neurounina treatment ameliorated motor symptoms and increased survival rate in SOD1 ^{G93A} mice

To investigate whether the reduced loss of MNs observed in neurounina treated SOD1^{G93A} mice was accompanied by an amelioration of the motor performance of these mice, behavioral tests were weekly performed on Wt and SOD1^{G93A} mice, starting from the second month after birth (P60), when i.p. administration of neurounina started and when the mice were asymptomatic. All animals were assigned to four experimental groups: Wt + vehicle, Wt + neurounina, SOD1 ^{G93A} + vehicle and SOD1^{G93A}+ neurounina, and then weighed, subjected to rotarod test, grip test and observed to detect the disease onset.

3.6.1. Survival

Neurounina extended the lifespan of ALS mice (Fig. 7). In fact, the average lifespan of SOD1 ^{G93A} mice treated with vehicle was 127.9 ± 1.65 days, while that of ALS mice treated with neurounina was significantly longer, being 146.2 ± 3 days (Fig. 7A).

3.6.2. Paralysis onset

The onset of the disease was defined when denervation-induced muscle atrophy produced 15–20% of the decline in motor performance in grip strength test. Indeed, the paralysis onset in SOD1^{G93A} treated with vehicle was 33.69 ± 1.31 days while in neurounina treated SOD1^{G93A} group was 42.47 ± 1.59 days (Fig. 7B).

3.6.3. Body weight

In vehicle SOD1^{G93A} mice the body weight loss was observed at 7 weeks after vehicle treatment both in female and male mice, indeed a 10% reduction in body weight was noted. On the other hand, in the group SOD1^{G93A} treated with neurounina for 8 weeks the weight remained stable over time. In fact, after 8 weeks of treatment with neurounina, body weight did not change compared to the group of Wt mice. In the group of females, at 7 weeks after neurounina treatment, weight loss was evident, but it was recovered the following week. No differences were observed between Wt mice treated with neurounina

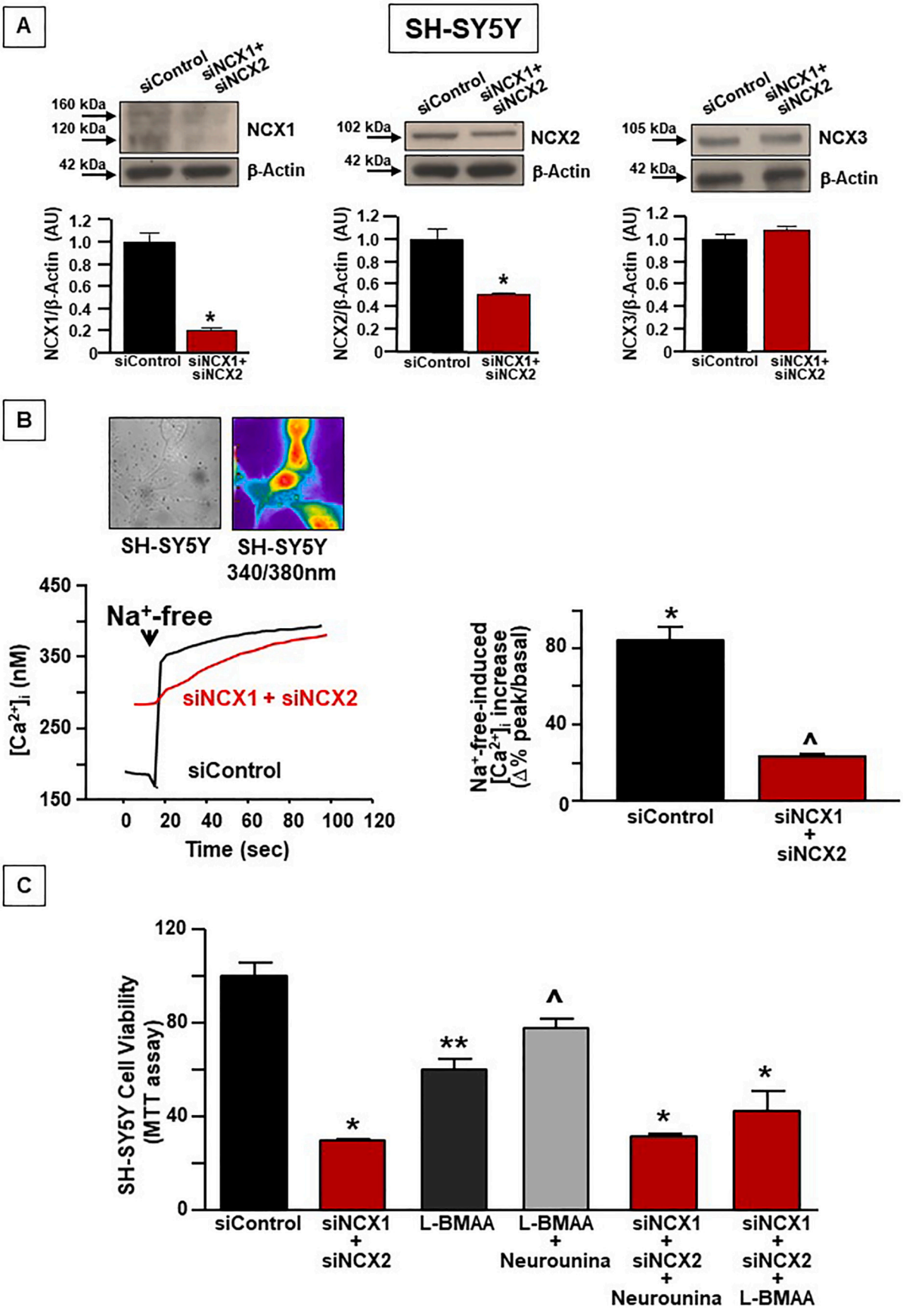

(caption on next page)

Fig. 4. Neurounina is not able to rescue L-BMAA induced cell toxicity in cell silenced for NCX1 and NCX2. (A) Representative Western blotting of NCX1 (left), NCX2 (middle) and NCX3 (right) proteins in the presence or absence of combo duplexes against NCX1 and NCX2 (on NCX1: siControl 1 and siNCX1 + siNCX2 0.2 ± 0.017; $p < 0.05$. On NCX2:siControl 1 and siNCX1 + siNCX2 0.51 ± 0.011; $p < 0.05$. On NCX3: siControl 1 and siNCX1 + siNCX2 1.077 ± 0.028). The experiments were repeated on three different preparations. (B) Representative images and traces of NCX activity, quantified as $[Ca^{2+}]i$ increase induced by Na^{+} −free perfusion in Fura-2 AM-loaded SH-SY5Y previously treated with siControl or with combo duplexes (siNCX1 + siNCX2). The experiments were repeated three times on almost 15 cells for each group. (C) Cell viability measured as MTT in SH-SY5Y treated with L-BMAA (2 mM/120 h in 0% FBS). The experiments were repeated at least three times on different cell preparations. *$p < 0.05$ vs all; **$p < 0.05$ vs siControl; ^$p < 0.05$ vs siControl and L-BMAA.

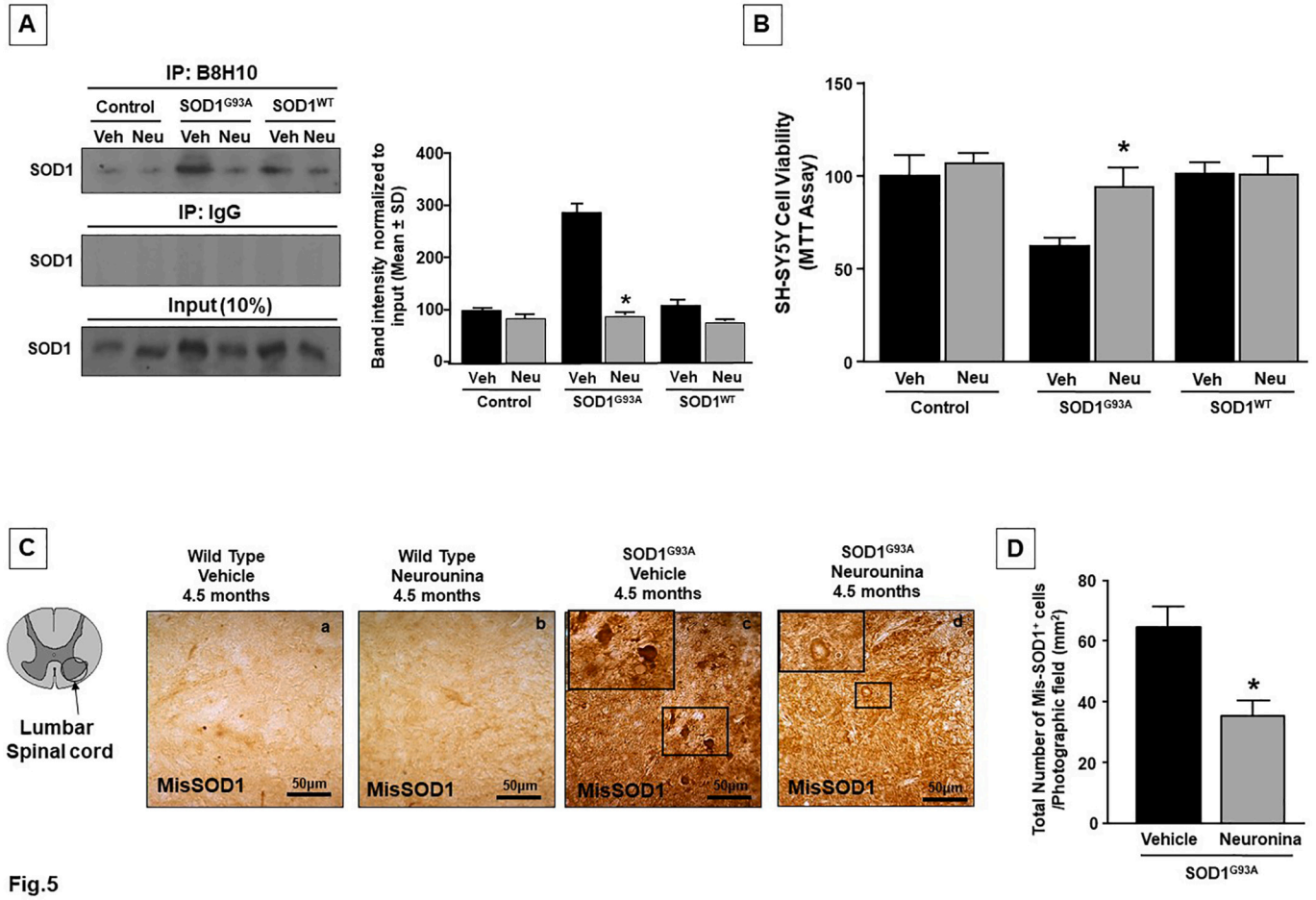

Fig.5

Fig. 5. Neurounina improves the survival of neurons expressing a mutant SOD1 by inhibiting the accumulation of misfolded SOD1. SH-SY5Y neuroblastoma cells have been transfected to express the human SOD1 Wild type ($SOD1^{WT}$), the human mutant SOD1-G93A ($SOD1^{G93A}$), or neither (Control), in each case either with neurounina or vehicle. (A-left) Misfolded SOD1 was detected by immunoblotting of immunoprecipitates produced with the B8H10 antibody, which recognizes only the misfolded forms of SOD1. (A-right) Quantitative analysis of the Co-Ip experiments normalized to input. (B) Cell viability analysis performed with MTT assay. Quantitative analysis from triplicate of different biological repeats (n = 3) was performed using one-way ANOVA. *$p < 0.05$ vs SOD^{G93A} + vehicle. (C a–d) DAB immunostaining of misfolded SOD1 with B8H10 antibody. Scale Bar 50 µm. In c,d High magnification 200× zoom. (D) Total number of misfolded SOD1 positive cells in vehicle $SOD1^{G93A}$ compared to neurounina $SOD1^{G93A}$ (n = 3 for each group) *t*-test *$p < 0.05$, $SOD1^{G93A}$ + vehicle vs $SOD1^{G93A}$ + neurounina.

and Wt mice treated with vehicle (Fig. 7C).

3.6.4. Rotarod test

Motor coordination of Wt and G93A mice treated with vehicle or with neurounina was assessed as the ability of mice to maintain balance on an accelerating rotarod at 1 through 8 weeks of vehicle or neurounina treatment. The wild type mice were able to maintain balance for the duration of each test and neurounina treatment did not disrupt this performance (Fig. 8A). The G93A mice became progressively impaired in motor coordination. There was no difference between G93A treatment groups during rotarod training and no statistically significant difference. Significantly, neurounina treatment blunted the decline in rotarod performance in the G93A mice. Performance of the vehicle treated G93A mice progressed from a slight impairment at 2 weeks of treatment to complete loss of the ability to maintain balance at 8 weeks of treatment (3.7 ± 1 s). In contrast, performance deteriorated at a slower rate with neurounina treatment, as reflected in significantly longer durations in the $SOD1^{G93A}$ mice treated with neurounina compared to vehicle treated animals at weeks 7–8. In fact, at 8 weeks, the neurounina treated $SOD1^{G93A}$ mice maintained the ability to balance on the rotarod for an average of 21.4 ± 5 s (Fig. 8A). The rotarod onset was also delayed in $SOD1^{G93A}$ mice chronically treated with neurounina. Indeed 50% of the animals started to fall off the rotarod around the 45th day of neurounina treatment while the $SOD1^{G93A}$ vehicle treated mice fell around the 30th day (Fig. 8B).

3.6.5. Grip-strength test

Hindlimb grip test was evaluated by placing the mouse on a grid upside-down and the latency to fall off the grid was measured up to a maximum of 60 s. In the vehicle $SOD1^{G93A}$ mice the loss of limbs

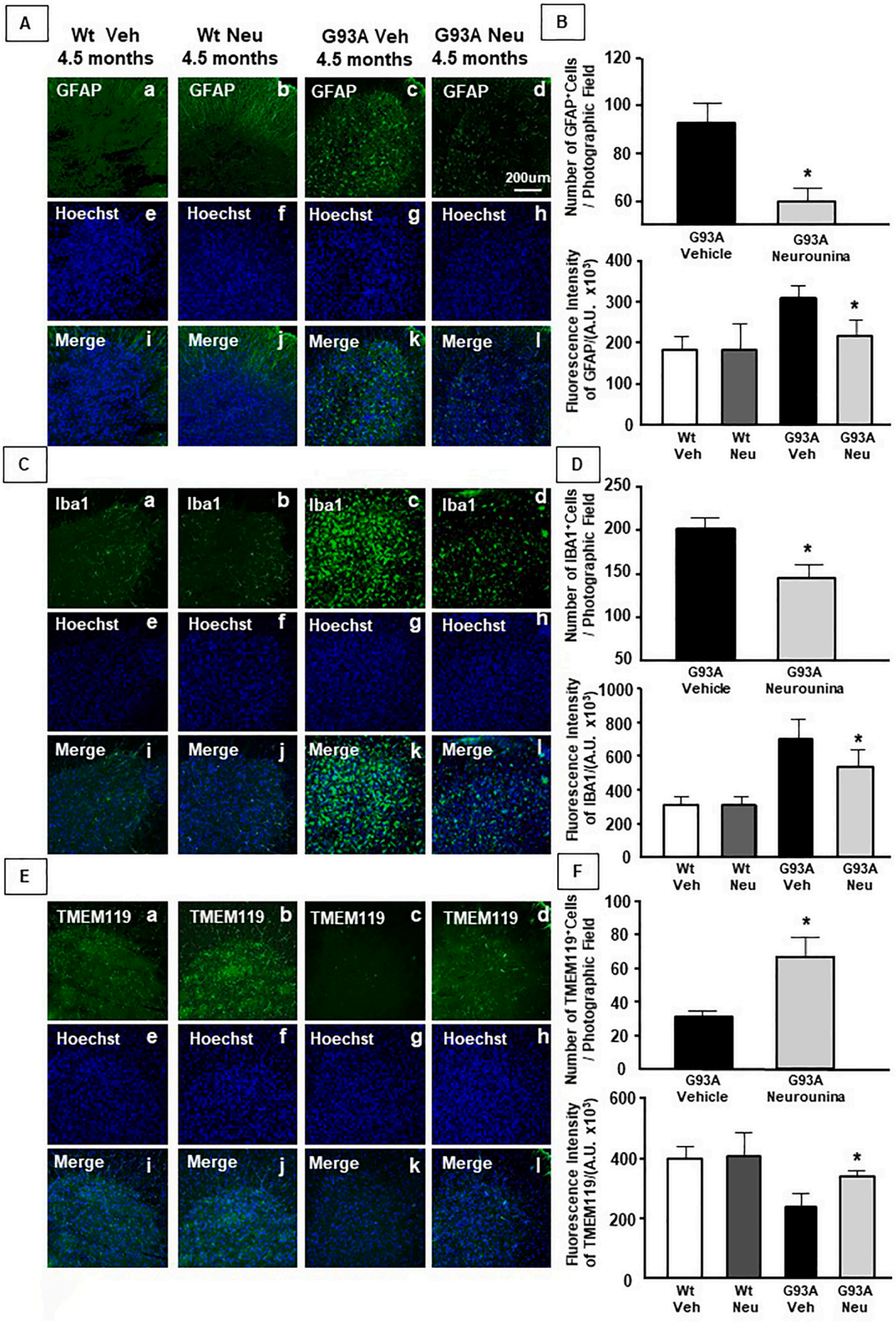

(caption on next page)

Fig. 6. Effect of neurounina on glia activation. (A) Immunofluorescence images showing (a,e,i) single labeling of GFAP in spinal cord of Wt mice treated with vehicle and (b,f,j) Wt mice treated with neurounina. (c,g,k) Single labeling of GFAP in spinal cord of $SOD1^{G93A}$ treated with Vehicle and (d,h,l) $SOD1^{G93A}$ treated with neurounina. (B) Total number of activated GFAP cells per photographic field (mm^2) and fluorescence intensity of GFAP labeling. (C a,e,i) single labeling of Iba1 in spinal cord of Wt mice treated with vehicle and (C b,f,j) Wt mice treated with neurounina. (C c,g,k) single labeling of Iba1 in spinal cord of $SOD1^{G93A}$ treated with Vehicle and (C d,h,l) $SOD1^{G93A}$ treated with neurounina. (D) Total number of activated Iba1 cells and Fluorescence intensity of Iba1 labeling per photographic field (mm^2). (E a,e,i) single labeling of TMEM119 in spinal cord of Wt mice treated with vehicle and (E b,f,j) Wt mice treated with neurounina. (E c,g,k) single labeling of TMEM119 in spinal cord of $SOD1^{G93A}$ treated with Vehicle and (E d,h,l) $SOD1^{G93A}$ treated with neurounina. (F) fluorescence intensity of TMEM119 labeling and fluorescence intensity of TMEM119 labeling. Scale bar 200 μm. Data are expressed as mean ± SEM (n = 3 for each group). *$p < 0.05$, SOD^{G93A}neurounina vs. SOD^{G93A} Vehicle. *P* values were obtained using t-test and one-way ANOVA with Newman Keuls's correction for multiple comparisons.

strength started evident after 6 weeks of treatment (28.8 ± 4 s), in fact the grip on the grid decreased by 50% compared to the Wt group. In ALS mice treated with neurounina the grip performance at 6 weeks was 43.8 ± 4 s and at 8 weeks the mice remained on the grid for another 20s (Fig. 8C). Finally, the onset of grip performance was improved in neurounina G93A mice, 50% of the animals started to lose their grip around the 45th day after treatment while the G93A vehicle mice fell around the 35th day (Fig. 8D).

4. Discussion

The results of this study clearly revealed that ALS mice showed a reduction in the expression and activity of NCX1 and of NCX2 in spinal cord, consistent with disease progression. In addition, we demonstrated that the pharmacological activation of NCX1 and NCX2 by the prolonged treatment of $SOD1^{G93A}$ mice with the newly synthesized compound neurounina: (1) prevented the reduction in NCX activity observed in spinal cord; (2) preserved MNs survival in the ventral spinal horn of $SOD1^{G93A}$ mice; (3) prevented the spinal cord accumulation of misfolded SOD1; (4) reduced astroglia and microglia activation and spared the resident microglia cells in the spinal cord; (5) improved the lifespan and mitigated motor symptoms of ALS mice.

These relevant effects due to NCX1 and NCX2 activation clearly indicate the importance, among other factors, of the correct functioning of Na^+ and Ca^{2+} clearance mechanisms in slowing down ALS progression. In fact, the key components of ALS pathophysiology include oxidative stress, excitotoxicity, mitochondrial dysfunctions and inflammatory processes (Appel, 2006; Appel et al., 2001). Notably, increased intracellular calcium, which is another identified pathological event, could merge these individual toxic mechanisms into a single, escalating and self-perpetuating cycle of neuronal degeneration (Siklos et al., 1996; Siklos et al., 1998). Over the years, several reports suggest that calcium homeostasis might be preserved by modulating the transmembrane calcium flux with therapeutic compounds or via altering the calcium binding protein content to maintain an enhanced calcium buffer capacity (Siklos et al., 1996; Siklos et al., 1998). Furthermore, defects linked to a low Ca^{2+}buffering ability represent a main risk factor (Appel et al., 2000; Berridge et al., 2003). Indeed, deficit or excess of calcium ions are linked to several pathological mechanisms (i.e. oxidative stress, excitotoxicity, immune/inflammatory processes, and mitochondrial dysfunction) which operate in an orchestrated way and amplify deleterious effects on MNs (Cozzolino et al., 2012). Proof of this is the fact that ALS patients show higher calcium levels both in muscle and in spinal cord neurons (Appel, 2006; Appel et al., 2001; Appel et al., 2000). In addition, oculomotor nerve, that is spared in ALS patients, is able to maintain the control of ionic homeostasis by overexpressing proteins and membrane transporters capable of buffering sodium and calcium overload, such as calbindin and paravalbumin (Appel, 2006; Appel et al., 2001; Appel et al., 2000; Jaiswal et al., 2009).

In the light of these premises, we investigated the involvement of the plasma membrane sodium/calcium exchanger in the pathogenesis of ALS and its possible "druggability". On the other hand, although there are still no approved drugs that act on NCX, the modulation of this antiporter has been successfully applied in numerous animal models of diseases of the CNS, such as Alzheimer's disease (Pannaccione et al., 2020; Pannaccione et al., 2012; Sokolow et al., 2011), multiple sclerosis (Boscia et al., 2012; Kurnellas et al., 2007); neonatal encephalopathy (Cerullo et al., 2018) and adult stroke (Annunziato et al., 2007; Molinaro et al., 2008; Pignataro et al., 2004; Pignataro et al., 2014). Notably, in our laboratory, the activity of the plasma membrane transporter Na^+/Ca^{2+} exchanger 3 (NCX3) has been linked to ALS pathophysiology (Anzilotti et al., 2018). In fact, it has been recently reported that the protective strategy known as preconditioning, induced by subthreshold doses of the neurotoxin L-BMAA, an aminoacid linked to ALS induction, is able to delay MNs degeneration and to prolong ALS mice survival also through the prevention of the reduction of NCX3 expression at muscle and CNS level, suggesting that this antiporter can represent a valuable pharmacological target to delay disease progression (Anzilotti et al., 2018). In fact, NCX3 is an NCX isoform present only in skeletal muscles and at lower levels of expression in selected brain regions (Quednau et al., 1997), while the other two nNCX gene products, NCX1 and NCX2 are widely expressed within the CNS (Canitano et al., 2002; Papa et al., 2003; Quednau et al., 1997).

These considerations prompted us to further investigate NCX isoforms contribution in the pathophysiology of ALS, with particular regard to NCX1 and NCX2. In fact, a significant down-regulation of NCX1 and NCX2 mRNA early during disease development, followed, later on, by protein down-regulation occurred. This time discrepancy could probably be due to several factors, such as different half-lives of mRNA and protein, an elevate translational rate of mRNA or to the presence of protein modifications that can affect their stability.

To prevent the reduction in NCX1 and NCX2 activity observed in $SOD1^{G93A}$ mice during the progression of the disease, the NCX1/NCX2 activator neurounina was daily intraperitoneally administered since the early symptomatic phase. The neuroprotective effects of neurounina were evident at molecular level as well as at behavioral levels, and were probably mediated also through accessory activities. In fact, neurounina, besides its effects on NCX activity, is also able to inhibit both glutamate release and NMDA receptors in cortical neurons (Molinaro et al., 2013). This effect represents a very important aspect in ALS pathophysiology, where glutamate excitotoxicity plays an important role (Van Damme et al., 2005). Indeed, several studies suggested that excitotoxicity occurring in MNs impairs the mitochondrial respiratory and contribute to MNs degeneration (Grosskreutz et al., 2010). These alterations lead to an increase in ROS production and a reduction in the glutamate uptake in glia cells with high levels of glutamate in the synaptic cleft and an increase in the calcium influx through Ca^{2+}−permeable glutamate receptor channels (Grosskreutz et al., 2010). Therefore, this evidence suggest that part of the neuroprotective effect of neurounina could be also attributed to a partial inhibition of both endogenous glutamate release and NMDA receptor activity.

It cannot be excluded an effect of neurounina also at axonal level. In this regard, the "dying-back theory" hypothesizes that axonal damage occurs early during the disease, before neuronal degeneration, and onset of symptoms (Fischer et al., 2004). Therefore, although the NCX activator neurounina was administered at the beginning of the symptomatic phase, when the axonal neurodegenerative process already started, its activation may slowdown the neurodegenerative process also at axonal level. On the other hand, in the present study we clearly demonstrated that NCX activation occurred also on soma motor neurons, where we showed a relevant presence of NCX signal by confocal microscopy.

It is also important to point out that the inflammatory reactions

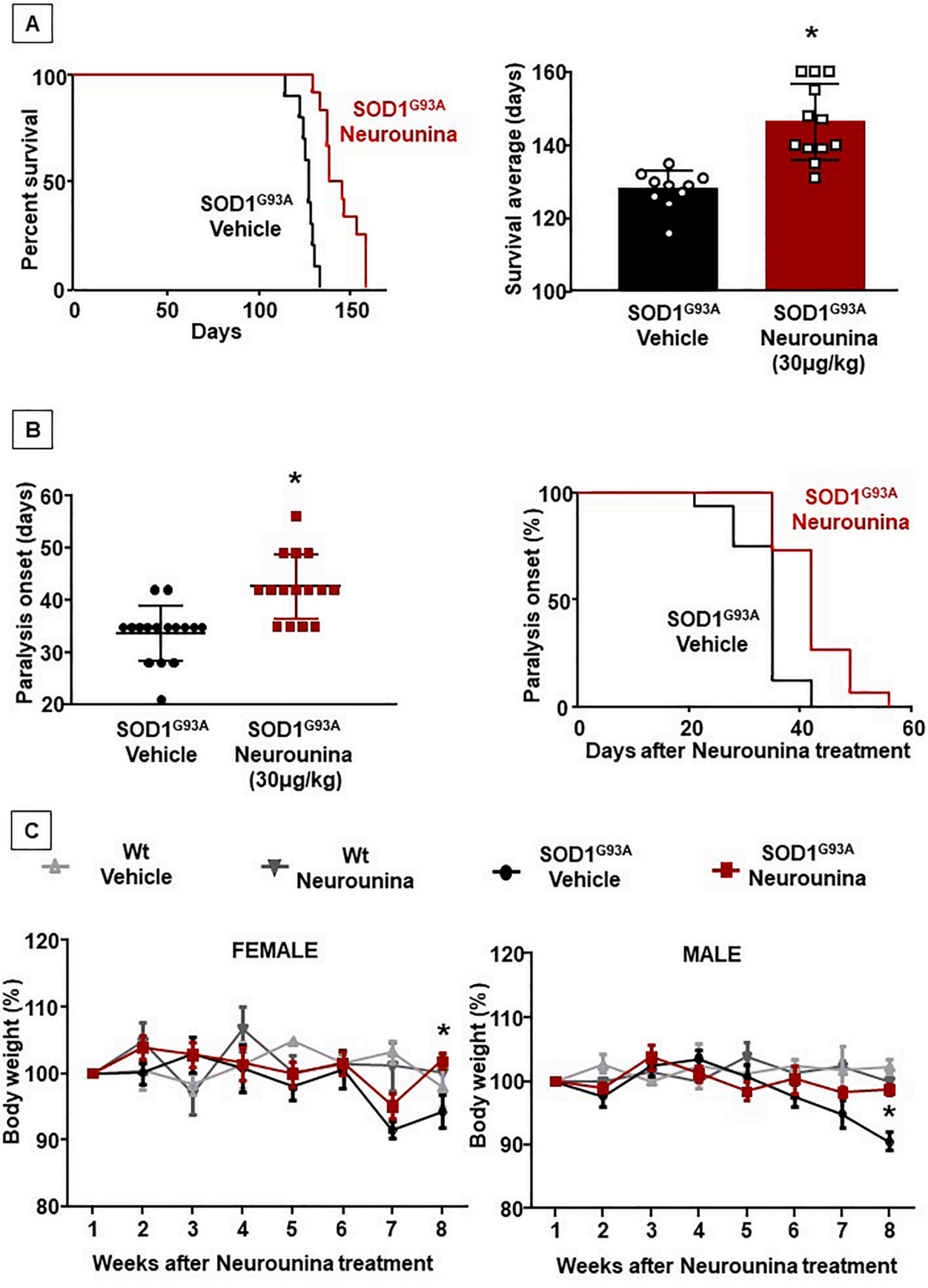

(caption on next page)

Fig. 7. Effect of neurounina on survival, paralysis onset and body weight reduction in SOD1^{G93A}mice. (A) Kaplan-Meier survival analysis, expressed as a percentage and in days, $n = 10$ SOD1^{G93A} mice treated with vehicle (white circle) and $n = 12$ SOD1^{G93A} treated with neurounina (white square). Statistical analysis was performed using a Student's *t*-Test; significant differences are indicated as: *p < 0.05, SOD1^{G93A}neurounina vs. SOD1^{G93A} Vehicle. (B) Paralysis onset analysis expressed in days or in percentage. $n = 14$ of SOD1^{G93A} treated with vehicle (black circle) and $n = 15$ of SOD1^{G93A} treated with neurounina (black square). Statistical analysis was performed using a Student's t-Test; significant differences are indicated as: *p < 0.05, SOD1^{G93A}neurounina vs. SOD1^{G93A} Vehicle. (C) Percentage of body weight reduction in Wt vehicle (n = 3 male and 3 female), Wteurounina (n = 3 male and 3 female) SOD1^{G93A} vehicle ($n = 7$ male and 9 female) and SOD1^{G93A} treated with neurounina (n = 7male and 8 female) mice. *P* values were obtained using one-way ANOVA with Newman Keuls's correction for multiple comparisons. *p < 0.05 SOD1^{G93A} vs. SOD1^{G93A}neurounina.

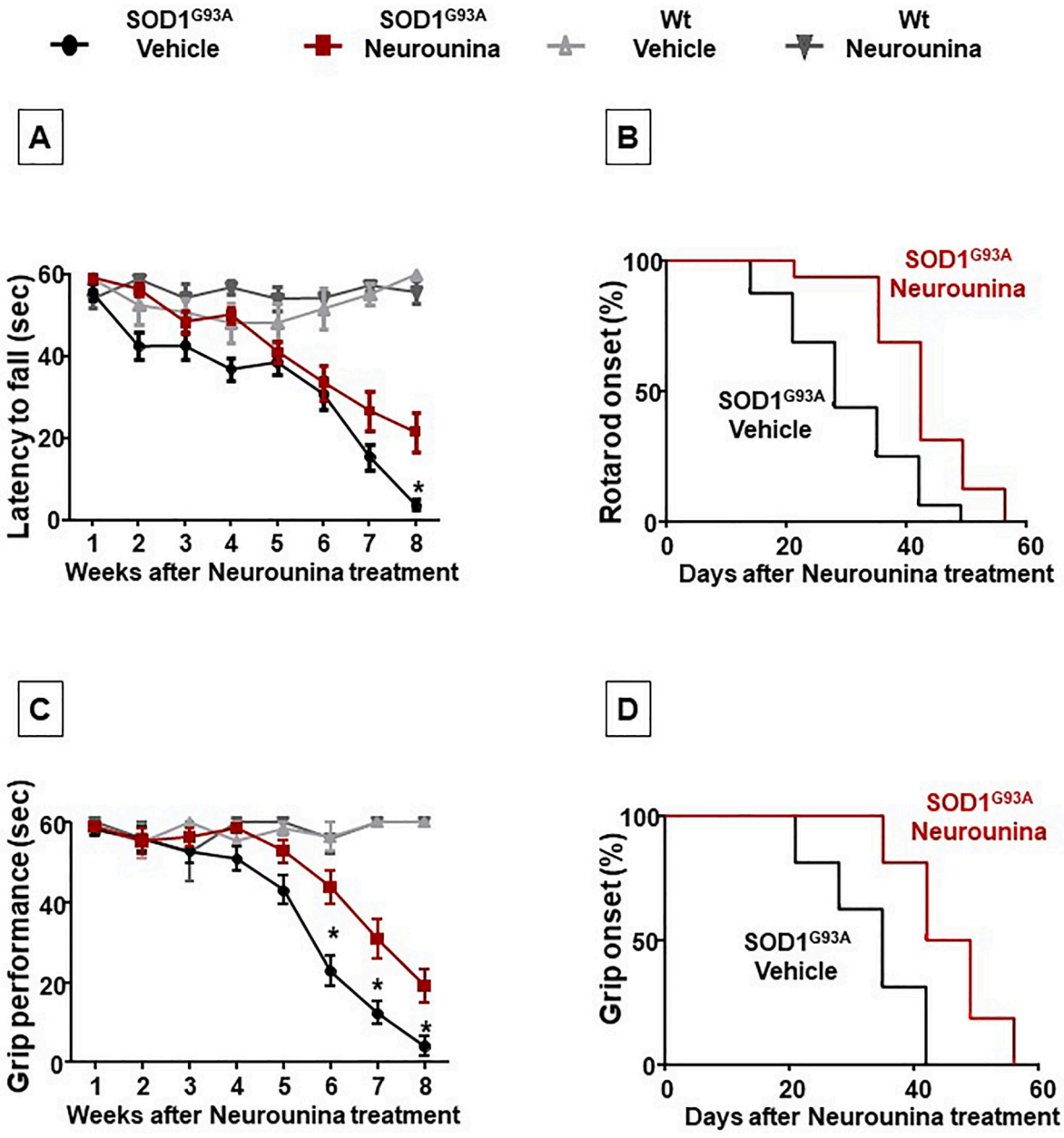

Fig. 8. Effect of neurounina on motor performances in SOD1^{G93A} mice. Rotarod test in panel (A) rotarod onset expressed as percentage in (B). Grip performance test in panel (C) and grip onset in (D). Wt vehicle (n = 6), Wt neurounina (n = 6) SOD1^{G93A} vehicle (n = 15) and SOD1 ^{G93A}neurounina (n = 14) mice. Significant differences are indicated as: *p < 0.05, SOD1^{G93A}neurounina vs. SOD1^{G93A} vehicle. *P* values were obtained using one-way ANOVA with Newman Keuls's correction for multiple comparisons.

mediated by astroglia and microglia cells, that are hallmarks of ALS pathology (Philips and Rothstein, 2014), are reduced in neurounina treated SOD1 mice. In astrocytes and in microglia cells all three NCX isoforms are expressed (Boscia et al., 2016), among the three NCX isoforms, NCX1 transcripts are the most highly represented (Pappalardo et al., 2014). In particular, the importance of NCX1 at microglial level is provided by the fact that *NCX1*$^{-/-}$ embryos have no detectable microglia in the brain (Ginhoux et al., 2010). In addition, studies performed *ex*

vivo, in microglia isolated from rat ischemic brain, and *in vitro*, in cultured microglia, suggest that a Na^+-dependent Ca^{2+} influx through NCX operating in the reverse mode is necessary for microglia activation (Boscia et al., 2009; Hoffman et al., 2003).

Furthermore, these anti-inflammatory effects could be due to the reduction of glutamate and the rebalancing of intracellular Ca^{2+} overload, thus leading to a lower MNs death and finally to a reduction in gliosis.

In addition, it is known that the increase in the intracellular Ca^{2+} concentrations disrupts the correct cellular protein folding machinery thus leading to an accumulation of misfolded SOD1 and eventual death of these neurons (Tateno et al., 2004). In this regard, we recently demonstrated that in NSC-34 motor neurons the presence of the mutant SOD1 induces a relevant increase of intracellular Ca^{2+} concentrations that leads to the aggregation of misfolded SOD1 (Petrozziello et al., 2017). In fact, Ca^{2+} ions can bind to SOD1 and induce conformational changes in its folding propensity, thus determining aggregation (Leal et al., 2013). In addition, reducing intracellular Ca^{2+} overload has been linked to an attenuation of SOD1 aggregation (Parone et al., 2013). As Na^+/Ca^{2+} exchanger one of the major player in mediating Ca^{2+} efflux / Na^+ influx (forward mode of operation), when the bivalent cation is elevated in the cytosol, it is plausible to hypothesize that NCX stimulation by neurounina may reduce SOD1 aggregation through the reduction of intracellular Ca^{2+} level consequent to NCX working in the forward mode of operation (Sirabella et al., 2018).

More importantly, we found that prolonged *in vivo* neurounina treatment, through NCX1 and NCX2 activation could be considered an effective strategy for ALS. Indeed, this NCX activator, by enhancing NCX1 and NCX2 activity, improved motor skills and survival of $SOD1^{G93A}$ mice, underlining that the maintenance of sodium and calcium homeostasis might represent a pivotal mechanism for MNs survival.

Relevantly, preclinical neurounina studies showed that neurounina is provided with a high lipophilicity index, low toxicity and ability to cross BBB when systemically administered (Severino et al., 2019). Furthermore, neurounina displays *in vitro* a potent and reversible stimulatory effect on NCX1 and NCX2 in both forward and reverse modes of operation, with an estimated EC_{50} in the low nanomolar ranges. In consideration of alls these pharmacokinetic, pharmacodynamic and toxicological properties, it is possible to hypothesize a future transability of the present study to human pathology.

Supplementary data to this article can be found online at https://doi.org/10.1016/j.nbd.2021.105480.

Conflicts of Interest

"Nothing to report."

Anzilotti Serenella, Conceptualization, Immunoistochemistry experiments, Data curation, Original draft preparation.

Valsecchi Valeria, RT-PCR and Western Blotting Experiments.

Brancaccio Paola, Hassler Brenda, Cuomo Ornella, Immunoistochemistry experiments, Behavioral experiments.

Guida Natascia and Laudati Giusy, SOD1 Misfolded Aggregation experiments.

Tedeschi Valentina, Petrozziello Tiziana and Secondo Agnese, Synaptosomal preparations, Ca^{2+} imaging, Cell viability after siRNA treatment.

Frecentese Francesco and Magli Elisa, Drug preparations and dosage setting.

Formisano Luigi and Secondo Agnese, Data analysis, Reviewing and Editing.

Annunziato Lucio and Pignataro Giuseppe, Supervision, Conceptualization, Writing, Reviewing and Editing.

Acknowledgement

We thank Dr. Lucia d'Esposito for her invaluable support in all *in vivo* studies. This work was supported by grants from Programma Operativo Nazionale (PON PERMEDNET ArSol-1226) from the Italian Ministry of Research, MIUR, to L.A.; BIGIMAGING from Italian Ministry of Economic Development to GP and PON NEON (ARS01_00769) from the Italian Ministry of Research, MIUR, to GP.

References

Amoroso, S., Tortiglione, A., Secondo, A., Catalano, A., Montagnani, S., Di Renzo, G., Annunziato, L., 2000. Sodium nitroprusside prevents chemical hypoxia-induced cell death through iron ions stimulating the activity of the Na+-Ca2+ exchanger in C6 glioma cells. J. Neurochem. 74 (4), 1505–1513. https://doi.org/10.1046/j.1471-4159.2000.0741505.x.

Annunziato, L., Pignataro, G., Boscia, F., Sirabella, R., Formisano, L., Saggese, M., Di Renzo, G.F., 2007. ncx1, ncx2, and ncx3 gene product expression and function in neuronal anoxia and brain ischemia. Ann. N. Y. Acad. Sci. 1099, 413–426. https://doi.org/10.1196/annals.1387.050.

Anzilotti, S., Tornincasa, M., Gerlini, R., Conte, A., Brancaccio, P., Cuomo, O., Pierantoni, G.M., 2015. Genetic ablation of homeodomain-interacting protein kinase 2 selectively induces apoptosis of cerebellar Purkinje cells during adulthood and generates an ataxic-like phenotype. Cell Death Dis. 6, e2004 https://doi.org/10.1038/cddis.2015.298.

Anzilotti, S., Brancaccio, P., Simeone, G., Valsecchi, V., Vinciguerra, A., Secondo, A., Pignataro, G., 2018. Preconditioning, induced by sub-toxic dose of the neurotoxin L-BMAA, delays ALS progression in mice and prevents Na(+)/Ca(2+) exchanger 3 downregulation. Cell Death Dis. 9 (2), 206. https://doi.org/10.1038/s41419-017-0227-9.

Appel, S.H., 2006. Is ALS a systemic disorder? Evidence from muscle mitochondria. Exp. Neurol. 198 (1), 1–3. https://doi.org/10.1016/j.expneurol.2005.12.025.

Appel, S.H., Beers, D., Smith, R.G., Wilson, J.E., 2000. Altered calcium homeostasis in ALS as a target for therapy. Amyotroph Lateral Scler. Other Motor Neuron. Disord. 1 (Suppl. 4), 27–32.

Appel, S.H., Beers, D., Siklos, L., Engelhardt, J.I., Mosier, D.R., 2001. Calcium: the Darth Vader of ALS. Amyotroph Lateral Scler. Other Motor Neuron. Disord. 2 (Suppl. 1), S47–S54.

Berridge, M.J., Bootman, M.D., Roderick, H.L., 2003. Calcium signalling: dynamics, homeostasis and remodelling. Nat. Rev. Mol. Cell Biol. 4 (7), 517–529. https://doi.org/10.1038/nrm1155.

Blaustein, M.P., Lederer, W.J., 1999. Sodium/calcium exchange: its physiological implications. Physiol. Rev. 79 (3), 763–854. https://doi.org/10.1152/physrev.1999.79.3.763.

Boscia, F., Gala, R., Pannaccione, A., Secondo, A., Scorziello, A., Di Renzo, G., Annunziato, L., 2009. NCX1 expression and functional activity increase in microglia invading the infarct core. Stroke 40 (11), 3608–3617. https://doi.org/10.1161/STROKEAHA.109.557439.

Boscia, F., D'Avanzo, C., Pannaccione, A., Secondo, A., Casamassa, A., Formisano, L., Annunziato, L., 2012. Silencing or knocking out the Na(+)/Ca(2+) exchanger-3 (NCX3) impairs oligodendrocyte differentiation. Cell Death Differ. 19 (4), 562–572. https://doi.org/10.1038/cdd.2011.125.

Canitano, A., Papa, M., Boscia, F., Castaldo, P., Sellitti, S., Taglialatela, M., Annunziato, L., 2002. Brain distribution of the Na+/Ca2+ exchanger-encoding genes NCX1, NCX2, and NCX3 and their related proteins in the central nervous system. Ann. N. Y. Acad. Sci. 976, 394–404. https://doi.org/10.1111/j.1749-6632.2002.tb04766.x.

Cantarella, G., Pignataro, G., Di Benedetto, G., Anzilotti, S., Vinciguerra, A., Cuomo, O., Bernardini, R., 2014. Ischemic tolerance modulates TRAIL expression and its receptors and generates a neuroprotected phenotype. Cell Death Dis. 5, e1331 https://doi.org/10.1038/cddis.2014.286 (cddis2014286 [pii]).

Cerullo, P., Brancaccio, P., Anzilotti, S., Vinciguerra, A., Cuomo, O., Fiorino, F., Pignataro, G., 2018. Acute and long-term NCX activation reduces brain injury and restores behavioral functions in mice subjected to neonatal brain ischemia. Neuropharmacology 135, 180–191 doi:S0028-3908(18)30128-X [pii]. https://doi.org/10.1016/j.neuropharm.2018.03.017.

Coda, A.R., Anzilotti, S., Boscia, F., Greco, A., Panico, M., Gargiulo, S., Pappata, S., 2021. In vivo imaging of CNS microglial activation/macrophage infiltration with combined [(18)F]DPA-714-PET and SPIO-MRI in a mouse model of relapsing remitting experimental autoimmune encephalomyelitis. Eur. J. Nucl. Med. Mol. Imaging 48 (1), 40–52. https://doi.org/10.1007/s00259-020-04842-7.

Cozzolino, M., Pesaresi, M.G., Gerbino, V., Grosskreutz, J., Carri, M.T., 2012. Amyotrophic lateral sclerosis: new insights into underlying molecular mechanisms and opportunities for therapeutic intervention. Antioxid. Redox Signal. 17 (9), 1277–1330. https://doi.org/10.1089/ars.2011.4328.

Cuomo, O., Vinciguerra, A., Cerullo, P., Anzilotti, S., Brancaccio, P., Bilo, L., Pignataro, G., 2015. Ionic homeostasis in brain conditioning. Front. Neurosci. 9, 277. https://doi.org/10.3389/fnins.2015.00277.

Fischer, L.R., Culver, D.G., Tennant, P., Davis, A.A., Wang, M., Castellano-Sanchez, A., … Glass, J.D., 2004. Amyotrophic lateral sclerosis is a distal axonopathy: evidence in mice and man. Exp. Neurol. 185 (2), 232–240. https://doi.org/10.1016/j.expneurol.2003.10.004.

Formisano, L., Guida, N., Valsecchi, V., Pignataro, G., Vinciguerra, A., Pannaccione, A., Secondo, A., Boscia, F., Molinaro, P., Sisalli, M.J., Sirabella, R., Casamassa, A., Canzoniero, L.M., Di Renzo, G., Annunziato, L., 2013 Feb. NCX1 is a new rest target gene: role in cerebral ischemia. Neurobiol Dis. 50, 76–85. https://doi.org/10.1016/j.nbd.2012.10.010. Epub 2012 Oct 13. PMID: 23069678.

Gargiulo, S., Anzilotti, S., Coda, A.R., Gramanzini, M., Greco, A., Panico, M., Pappata, S., 2016. Imaging of brain TSPO expression in a mouse model of amyotrophic lateral sclerosis with (18)F-DPA-714 and micro-PET/CT. Eur. J. Nucl. Med. Mol. Imaging 43 (7), 1348–1359. https://doi.org/10.1007/s00259-016-3311-y.

Ginhoux, F., Greter, M., Leboeuf, M., Nandi, S., See, P., Gokhan, S., Merad, M., 2010. Fate mapping analysis reveals that adult microglia derive from primitive macrophages. Science 330 (6005), 841–845. https://doi.org/10.1126/science.1194637.

Grosskreutz, J., Van Den Bosch, L., Keller, B.U., 2010. Calcium dysregulation in amyotrophic lateral sclerosis. Cell Calcium 47 (2), 165–174. https://doi.org/10.1016/j.ceca.2009.12.002.

Grynkiewicz, G., Poenie, M., Tsien, R.Y., 1985 Mar 25. A new generation of Ca2+ indicators with greatly improved fluorescence properties. J Biol Chem 260 (6), 3440–3450. PMID: 3838314.

Guerini, D., Coletto, L., Carafoli, E., 2005. Exporting calcium from cells. Cell Calcium 38 (3–4), 281–289. https://doi.org/10.1016/j.ceca.2005.06.032.

Guida, N., Laudati, G., Mascolo, L., Valsecchi, V., Sirabella, R., Selleri, C., Formisano, L., 2017. p38/Sp1/Sp4/HDAC4/BDNF axis is a novel molecular pathway of the neurotoxic effect of the methylmercury. Front. Neurosci. 11, 8. https://doi.org/10.3389/fnins.2017.00008.

Hand, C.K., Khoris, J., Salachas, F., Gros-Louis, F., Lopes, A.A., Mayeux-Portas, V., Rouleau, G.A., 2002. A novel locus for familial amyotrophic lateral sclerosis, on chromosome 18q. Am. J. Hum. Genet. 70 (1), 251–256. https://doi.org/10.1086/337945.

Hoffman, J.R., Greenberg, J.H., Furuya, D., Craik, R.L., Fanelli, P., Breslow, S., Hand, P., 2003. Rats recovering from unilateral barrel-cortex ischemia are capable of completing a whisker-dependent task using only their affected whiskers. Brain Res. 965 (1–2), 91–99. https://doi.org/10.1016/s0006-8993(02)04141-0.

Jaiswal, M.K., 2019. Riluzole and edaravone: a tale of two amyotrophic lateral sclerosis drugs. Med. Res. Rev. 39 (2), 733–748. https://doi.org/10.1002/med.21528.

Jaiswal, M.K., Zech, W.D., Goos, M., Leutbecher, C., Ferri, A., Zippelius, A., Keller, B.U., 2009. Impairment of mitochondrial calcium handling in a mtSOD1 cell culture model of motoneuron disease. BMC Neurosci. 10, 64. https://doi.org/10.1186/1471-2202-10-64.

Kurnellas, M.P., Donahue, K.C., Elkabes, S., 2007. Mechanisms of neuronal damage in multiple sclerosis and its animal models: role of calcium pumps and exchangers. Biochem. Soc. Trans. 35 (Pt 5), 923–926. https://doi.org/10.1042/BST0350923.

Laudati, G., Mascolo, L., Guida, N., Sirabella, R., Pizzorusso, V., Bruzzaniti, S., Formisano, L., 2019. Resveratrol treatment reduces the vulnerability of SH-SY5Y cells and cortical neurons overexpressing SOD1-G93A to thimerosal toxicity through SIRT1/DREAM/PDYN pathway. Neurotoxicology 71, 6–15. https://doi.org/10.1016/j.neuro.2018.11.009.

Leal, S.S., Cardoso, I., Valentine, J.S., Gomes, C.M., 2013. Calcium ions promote superoxide dismutase 1 (SOD1) aggregation into non-fibrillar amyloid: a link to toxic effects of calcium overload in amyotrophic lateral sclerosis (ALS)? J. Biol. Chem. 288 (35), 25219–25228. https://doi.org/10.1074/jbc.M113.470740.

Leyton-Jaimes, M.F., Benaim, C., Abu-Hamad, S., Kahn, J., Guetta, A., Bucala, R., Israelson, A., 2016. Endogenous macrophage migration inhibitory factor reduces the accumulation and toxicity of misfolded SOD1 in a mouse model of ALS. Proc. Natl. Acad. Sci. U. S. A. 113 (36), 10198–10203. https://doi.org/10.1073/pnas.1604600113.

Molinaro, P., Cuomo, O., Pignataro, G., Boscia, F., Sirabella, R., Pannaccione, A., Annunziato, L., 2008. Targeted disruption of Na+/Ca2+ exchanger 3 (NCX3) gene leads to a worsening of ischemic brain damage. J. Neurosci. 28 (5), 1179–1184. https://doi.org/10.1523/JNEUROSCI.4671-07.2008.

Molinaro, P., Cantile, M., Cuomo, O., Secondo, A., Pannaccione, A., Ambrosino, P., Annunziato, L., 2013. Neurounina-1, a novel compound that increases Na+/Ca2+ exchanger activity, effectively protects against stroke damage. Mol. Pharmacol. 83 (1), 142–156. https://doi.org/10.1124/mol.112.080986.

Natale, S., Anzilotti, S., Petrozziello, T., Ciccone, R., Serani, A., Calabrese, L., Molinaro, P., 2020. Genetic up-regulation or pharmacological activation of the Na(+)/Ca(2+) exchanger 1 (NCX1) enhances hippocampal-dependent contextual and spatial learning and memory. Mol. Neurobiol. https://doi.org/10.1007/s12035-020-01888-4.

Pannaccione, A., Secondo, A., Molinaro, P., D'Avanzo, C., Cantile, M., Esposito, A., Annunziato, L., 2012. A new concept: abeta1-42 generates a hyperfunctional proteolytic NCX3 fragment that delays caspase-12 activation and neuronal death. J. Neurosci. 32 (31), 10609–10617. https://doi.org/10.1523/JNEUROSCI.6429-11.2012.

Pannaccione, A., Piccialli, I., Secondo, A., Ciccone, R., Molinaro, P., Boscia, F., Annunziato, L., 2020. The Na(+)/Ca(2+)exchanger in Alzheimer's disease. Cell Calcium 87, 102190. https://doi.org/10.1016/j.ceca.2020.102190.

Papa, M., Canitano, A., Boscia, F., Castaldo, P., Sellitti, S., Porzig, H., Annunziato, L., 2003. Differential expression of the Na+-Ca2+ exchanger transcripts and proteins in rat brain regions. J. Comp. Neurol. 461 (1), 31–48. https://doi.org/10.1002/cne.10665.

Pappalardo, L.W., Samad, O.A., Black, J.A., Waxman, S.G., 2014. Voltage-gated sodium channel Nav 1.5 contributes to astrogliosis in an in vitro model of glial injury via reverse Na+ /Ca2+ exchange. Glia 62 (7), 1162–1175. https://doi.org/10.1002/glia.22671.

Parone, P.A., Da Cruz, S., Han, J.S., McAlonis-Downes, M., Vetto, A.P., Lee, S.K., Tseng, E., Cleveland, D.W., 2013. Enhancing mitochondrial calcium buffering capacity reduces aggregation of misfolded SOD1 and motor neuron cell death without extending survival in mouse models of inherited amyotrophic lateral sclerosis. J. Neurosci. 33 (11), 4657–4671. https://doi.org/10.1523/JNEUROSCI.1119-12.2013.

Pasinelli, P., Brown, R.H., 2006. Molecular biology of amyotrophic lateral sclerosis: insights from genetics. Nat. Rev. Neurosci. 7 (9), 710–723. https://doi.org/10.1038/nrn1971.

Petrozziello, T., Secondo, A., Tedeschi, V., Esposito, A., Sisalli, M., Scorziello, A., Annunziato, L., 2017. ApoSOD1 lacking dismutase activity neuroprotects motor neurons exposed to beta-methylamino-L-alanine through the Ca2+/Akt/ERK1/2 prosurvival pathway. Cell Death Differ. 24 (3), 511–522. https://doi.org/10.1038/cdd.2016.154.

Philips, T., Rothstein, J.D., 2014. Glial cells in amyotrophic lateral sclerosis. Exp. Neurol. (262 Pt B), 111–120. https://doi.org/10.1016/j.expneurol.2014.05.015.

Pignataro, G., Gala, R., Cuomo, O., Tortiglione, A., Giaccio, L., Castaldo, P., Annunziato, L., 2004. Two sodium/calcium exchanger gene products, NCX1 and NCX3, play a major role in the development of permanent focal cerebral ischemia. Stroke 35 (11), 2566–2570. https://doi.org/10.1161/01.str.0000143730.29964.93.

Pignataro, G., Sirabella, R., Anzilotti, S., Di Renzo, G., Annunziato, L., 2014. Does Na(+)/Ca(2)(+) exchanger, NCX, represent a new druggable target in stroke intervention? Transl. Stroke Res. 5 (1), 145–155. https://doi.org/10.1007/s12975-013-0308-8.

Pignataro, G., Ziaco, B., Tortiglione, A., Gala, R., Cuomo, O., Vinciguerra, A., Cataldi, M., 2015. Neuroprotective effect of VEGF-mimetic peptide QK in experimental brain ischemia induced in rat by middle cerebral artery occlusion. ACS Chem. Neurosci. 6 (9), 1517–1525. https://doi.org/10.1021/acschemneuro.5b00175.

Quednau, B.D., Nicoll, D.A., Philipson, K.D., 1997. Tissue specificity and alternative splicing of the Na+/Ca2+ exchanger isoforms NCX1, NCX2, and NCX3 in rat. Am. J. Phys. 272 (4 Pt 1), C1250–C1261. https://doi.org/10.1152/ajpcell.1997.272.4.C1250.

Rosen, D.R., Siddique, T., Patterson, D., Figlewicz, D.A., Sapp, P., Hentati, A., 1993. Mutations in Cu/Zn superoxide dismutase gene are associated with familial amyotrophic lateral sclerosis. Nature 362 (6415), 59–62. https://doi.org/10.1038/362059a0.

Secondo, A., Pignataro, G., Ambrosino, P., Pannaccione, A., Molinaro, P., Boscia, F., Annunziato, L., 2015. Pharmacological characterization of the newly synthesized 5-amino-N-butyl-2-(4-ethoxyphenoxy)-benzamide hydrochloride (BED) as a potent NCX3 inhibitor that worsens anoxic injury in cortical neurons, organotypic hippocampal cultures, and ischemic brain. ACS Chem. Neurosci. 6 (8), 1361–1370. https://doi.org/10.1021/acschemneuro.5b00043.

Severino, B., Corvino, A., Fiorino, F., Frecentese, F., Perissutti, E., Caliendo, G., De Nucci, G., 2019. Development, validation of LC-MS/MS method and determination of pharmacokinetic parameters of the stroke neuroprotectant neurounina-1 in beagle dog plasma after intravenous administration. Front. Pharmacol. 10, 432. https://doi.org/10.3389/fphar.2019.00432.

Siklos, L., Engelhardt, J., Harati, Y., Smith, R.G., Joo, F., Appel, S.H., 1996. Ultrastructural evidence for altered calcium in motor nerve terminals in amyotropic lateral sclerosis. Ann. Neurol. 39 (2), 203–216. https://doi.org/10.1002/ana.410390210.

Siklos, L., Engelhardt, J.I., Alexianu, M.E., Gurney, M.E., Siddique, T., Appel, S.H., 1998. Intracellular calcium parallels motoneuron degeneration in SOD-1 mutant mice. J. Neuropathol. Exp. Neurol. 57 (6), 571–587. https://doi.org/10.1097/00005072-199806000-00005.

Sirabella, R., Valsecchi, V., Anzilotti, S., Cuomo, O., Vinciguerra, A., Pignataro, G., 2018. Ionic homeostasis maintenance in ALS: focus on new therapeutic targets. Front. Neurosci. 7 (12), 510. https://doi.org/10.3389/fnins.2018.00510.

Sokolow, S., Luu, S.H., Headley, A.J., Hanson, A.Y., Kim, T., Miller, C.A., Gylys, K.H., 2011. High levels of synaptosomal Na(+)-Ca(2+) exchangers (NCX1, NCX2, NCX3) co-localized with amyloid-beta in human cerebral cortex affected by Alzheimer's disease. Cell Calcium 49 (4), 208–216. https://doi.org/10.1016/j.ceca.2010.12.008.

Tateno, M., Sadakata, H., Tanaka, M., Itohara, S., Shin, R.M., Miura, M., Takahashi, R., 2004. Calcium-permeable AMPA receptors promote misfolding of mutant SOD1 protein and development of amyotrophic lateral sclerosis in a transgenic mouse model. Hum. Mol. Genet. 13 (19), 2183–2196. https://doi.org/10.1093/hmg/ddh246.

Urbanczyk, J., Chernysh, O., Condrescu, M., Reeves, J.P., 2006 Sep 15. Sodium-calcium exchange does not require allosteric calcium activation at high cytosolic sodium concentrations. J Physiol 575 (Pt 3), 693–705. https://doi.org/10.1113/jphysiol.2006.113910. Epub 2006 Jun 29. PMID: 16809364; PMCID: PMC1995697.

Valsecchi, V., Boido, M., De Amicis, E., Piras, A., Vercelli, A., 2015. Expression of muscle-specific MiRNA 206 in the progression of disease in a murine SMA model. PLoS One 10 (6), e0128560. https://doi.org/10.1371/journal.pone.0128560.

Valsecchi, V., Anzilotti, S., Serani, A., Laudati, G., Brancaccio, P., Guida, N., Annunziato, L., 2020. miR-206 reduces the severity of motor neuron degeneration in the facial nuclei of the brainstem in a mouse model of SMA. Mol. Ther. https://doi.org/10.1016/j.ymthe.2020.01.013.

Van Damme, P., Dewil, M., Robberecht, W., Van Den Bosch, L., 2005. Excitotoxicity and amyotrophic lateral sclerosis. Neurodegener. Dis. 2 (3–4), 147–159. https://doi.org/10.1159/000089620.

Primary sources, secondary sources, and uncategorized references

Amoroso, S., Tortiglione, A., Secondo, A., Catalano, A., Montagnani, S., Di Renzo, G., Annunziato, L., 2000. Sodium nitroprusside prevents chemical hypoxia-induced cell death through iron ions stimulating the activity of the Na+-Ca2+ exchanger in C6

glioma cells. J. Neurochem. 74 (4), 1505–1513. https://doi.org/10.1046/j.1471-4159.2000.0741505.x.
Annunziato, L., Pignataro, G., Boscia, F., Sirabella, R., Formisano, L., Saggese, M., Di Renzo, G.F., 2007. ncx1, ncx2, and ncx3 gene product expression and function in neuronal anoxia and brain ischemia. Ann. N. Y. Acad. Sci. 1099, 413–426. https://doi.org/10.1196/annals.1387.050.
Anzilotti, S., Brancaccio, P., Simeone, G., Valsecchi, V., Vinciguerra, A., Secondo, A., Pignataro, G., 2018. Preconditioning, induced by sub-toxic dose of the neurotoxin L-BMAA, delays ALS progression in mice and prevents Na(+)/Ca(2+) exchanger 3 downregulation. Cell Death Dis. 9 (2), 206. https://doi.org/10.1038/s41419-017-0227-9.
Anzilotti, S., Tornincasa, M., Gerlini, R., Conte, A., Brancaccio, P., Cuomo, O., Pierantoni, G.M., 2015. Genetic ablation of homeodomain-interacting protein kinase 2 selectively induces apoptosis of cerebellar Purkinje cells during adulthood and generates an ataxic-like phenotype. Cell Death Dis. 6, e2004 https://doi.org/10.1038/cddis.2015.298.
Appel, S.H., 2006. Is ALS a systemic disorder? Evidence from muscle mitochondria. Exp. Neurol. 198 (1), 1–3. https://doi.org/10.1016/j.expneurol.2005.12.025.
Appel, S.H., Beers, D., Siklos, L., Engelhardt, J.I., Mosier, D.R., 2001. Calcium: the Darth Vader of ALS. Amyotroph Lateral Scler. Other Motor Neuron. Disord. 2 (Suppl. 1), S47–S54.
Appel, S.H., Beers, D., Smith, R.G., Wilson, J.E., 2000. Altered calcium homeostasis in ALS as a target for therapy. Amyotroph Lateral Scler. Other Motor Neuron. Disord. 1 (Suppl. 4), 27–32.
Berridge, M.J., Bootman, M.D., Roderick, H.L., 2003. Calcium signalling: dynamics, homeostasis and remodelling. Nat. Rev. Mol. Cell Biol. 4 (7), 517–529. https://doi.org/10.1038/nrm1155.
Blaustein, M.P., Lederer, W.J., 1999. Sodium/calcium exchange: its physiological implications. Physiol. Rev. 79 (3), 763–854. https://doi.org/10.1152/physrev.1999.79.3.763.
Boscia, F., Gala, R., Pannaccione, A., Secondo, A., Scorziello, A., Di Renzo, G., Annunziato, L., 2009. NCX1 expression and functional activity increase in microglia invading the infarct core. Stroke 40 (11), 3608–3617. https://doi.org/10.1161/STROKEAHA.109.557439.
Boscia, F., D'Avanzo, C., Pannaccione, A., Secondo, A., Casamassa, A., Formisano, L., Annunziato, L., 2012. Silencing or knocking out the Na(+)/Ca(2+) exchanger-3 (NCX3) impairs oligodendrocyte differentiation. Cell Death Differ. 19 (4), 562–572. https://doi.org/10.1038/cdd.2011.125.
Boscia, F., Begum, G., Pignataro, G., Sirabella, R., Cuomo, O., Casamassa, A., Sun, D., Annunziato, L., 2016 Oct. Glial Na(+) -dependent ion transporters in pathophysiological conditions. Glia 64 (10), 1677–1697. https://doi.org/10.1002/glia.23030. Epub 2016 Jul 26. PMID: 27458821; PMCID: PMC5238576.
Canitano, A., Papa, M., Boscia, F., Castaldo, P., Sellitti, S., Taglialatela, M., Annunziato, L., 2002. Brain distribution of the Na+/Ca2+ exchanger-encoding genes NCX1, NCX2, and NCX3 and their related proteins in the central nervous system. Ann. N. Y. Acad. Sci. 976, 394–404. https://doi.org/10.1111/j.1749-6632.2002.tb04766.x.
Cantarella, G., Pignataro, G., Di Benedetto, G., Anzilotti, S., Vinciguerra, A., Cuomo, O., Bernardini, R., 2014. Ischemic tolerance modulates TRAIL expression and its receptors and generates a neuroprotected phenotype. Cell Death Dis. 5, e1331 https://doi.org/10.1038/cddis.2014.286 (cddis2014286 [pii]).
Cerullo, P., Brancaccio, P., Anzilotti, S., Vinciguerra, A., Cuomo, O., Fiorino, F., Pignataro, G., 2018. Acute and long-term NCX activation reduces brain injury and restores behavioral functions in mice subjected to neonatal brain ischemia. Neuropharmacology 135, 180–191. https://doi.org/10.1016/j.neuropharm.2018.03.017.
Coda, A.R., Anzilotti, S., Boscia, F., Greco, A., Panico, M., Gargiulo, S., Pappata, S., 2021. In vivo imaging of CNS microglial activation/macrophage infiltration with combined [(18)F]DPA-714-PET and SPIO-MRI in a mouse model of relapsing remitting experimental autoimmune encephalomyelitis. Eur. J. Nucl. Med. Mol. Imaging 48 (1), 40–52. https://doi.org/10.1007/s00259-020-04842-7.
Cozzolino, M., Pesaresi, M.G., Gerbino, V., Grosskreutz, J., Carri, M.T., 2012. Amyotrophic lateral sclerosis: new insights into underlying molecular mechanisms and opportunities for therapeutic intervention. Antioxid. Redox Signal. 17 (9), 1277–1330. https://doi.org/10.1089/ars.2011.4328.
Cuomo, O., Vinciguerra, A., Cerullo, P., Anzilotti, S., Brancaccio, P., Bilo, L., Pignataro, G., 2015. Ionic homeostasis in brain conditioning. Front. Neurosci. 9, 277. https://doi.org/10.3389/fnins.2015.00277.
Gargiulo, S., Anzilotti, S., Coda, A.R., Gramanzini, M., Greco, A., Panico, M., Pappata, S., 2016. Imaging of brain TSPO expression in a mouse model of amyotrophic lateral sclerosis with (18)F-DPA-714 and micro-PET/CT. Eur. J. Nucl. Med. Mol. Imaging 43 (7), 1348–1359. https://doi.org/10.1007/s00259-016-3311-y.
Ginhoux, F., Greter, M., Leboeuf, M., Nandi, S., See, P., Gokhan, S., Merad, M., 2010. Fate mapping analysis reveals that adult microglia derive from primitive macrophages. Science 330 (6005), 841–845. https://doi.org/10.1126/science.1194637.
Grosskreutz, J., Van Den Bosch, L., Keller, B.U., 2010. Calcium dysregulation in amyotrophic lateral sclerosis. Cell Calcium 47 (2), 165–174. https://doi.org/10.1016/j.ceca.2009.12.002.
Guerini, D., Coletto, L., Carafoli, E., 2005. Exporting calcium from cells. Cell Calcium 38 (3–4), 281–289. https://doi.org/10.1016/j.ceca.2005.06.032.
Guida, N., Laudati, G., Mascolo, L., Valsecchi, V., Sirabella, R., Selleri, C., Formisano, L., 2017. p38/Sp1/Sp4/HDAC4/BDNF axis is a novel molecular pathway of the neurotoxic effect of the methylmercury. Front. Neurosci. 11, 8. https://doi.org/10.3389/fnins.2017.00008.
Hand, C.K., Khoris, J., Salachas, F., Gros-Louis, F., Lopes, A.A., Mayeux-Portas, V., Rouleau, G.A., 2002. A novel locus for familial amyotrophic lateral sclerosis, on chromosome 18q. Am. J. Hum. Genet. 70 (1), 251–256. https://doi.org/10.1086/337945.
Hoffman, J.R., Greenberg, J.H., Furuya, D., Craik, R.L., Fanelli, P., Breslow, S., Hand, P., 2003. Rats recovering from unilateral barrel-cortex ischemia are capable of completing a whisker-dependent task using only their affected whiskers. Brain Res. 965 (1–2), 91–99. https://doi.org/10.1016/s0006-8993(02)04141-0.
Jaiswal, M.K., 2019. Riluzole and edaravone: a tale of two amyotrophic lateral sclerosis drugs. Med. Res. Rev. 39 (2), 733–748. https://doi.org/10.1002/med.21528.
Jaiswal, M.K., Zech, W.D., Goos, M., Leutbecher, C., Ferri, A., Zippelius, A., Keller, B.U., 2009. Impairment of mitochondrial calcium handling in a mtSOD1 cell culture model of motoneuron disease. BMC Neurosci. 10, 64. https://doi.org/10.1186/1471-2202-10-64.
Kurnellas, M.P., Donahue, K.C., Elkabes, S., 2007. Mechanisms of neuronal damage in multiple sclerosis and its animal models: role of calcium pumps and exchangers. Biochem. Soc. Trans. 35 (Pt 5), 923–926. https://doi.org/10.1042/BST0350923.
Laudati, G., Mascolo, L., Guida, N., Sirabella, R., Pizzorusso, V., Bruzzaniti, S., Formisano, L., 2019. Resveratrol treatment reduces the vulnerability of SH-SY5Y cells and cortical neurons overexpressing SOD1-G93A to thimerosal toxicity through SIRT1/DREAM/PDYN pathway. Neurotoxicology 71, 6–15. https://doi.org/10.1016/j.neuro.2018.11.009.
Leyton-Jaimes, M.F., Benaim, C., Abu-Hamad, S., Kahn, J., Guetta, A., Bucala, R., Israelson, A., 2016. Endogenous macrophage migration inhibitory factor reduces the accumulation and toxicity of misfolded SOD1 in a mouse model of ALS. Proc. Natl. Acad. Sci. U. S. A. 113 (36), 10198–10203. https://doi.org/10.1073/pnas.1604600113.
Molinaro, P., Cantile, M., Cuomo, O., Secondo, A., Pannaccione, A., Ambrosino, P., Annunziato, L., 2013. Neurounina-1, a novel compound that increases Na+/Ca2+ exchanger activity, effectively protects against stroke damage. Mol. Pharmacol. 83 (1), 142–156. https://doi.org/10.1124/mol.112.080986.
Molinaro, P., Cuomo, O., Pignataro, G., Boscia, F., Sirabella, R., Pannaccione, A., Annunziato, L., 2008. Targeted disruption of Na+/Ca2+ exchanger 3 (NCX3) gene leads to a worsening of ischemic brain damage. J. Neurosci. 28 (5), 1179–1184. https://doi.org/10.1523/JNEUROSCI.4671-07.2008.
Natale, S., Anzilotti, S., Petrozziello, T., Ciccone, R., Serani, A., Calabrese, L., Molinaro, P., 2020. Genetic up-regulation or pharmacological activation of the Na(+)/Ca(2+) exchanger 1 (NCX1) enhances hippocampal-dependent contextual and spatial learning and memory. Mol. Neurobiol. https://doi.org/10.1007/s12035-020-01888-4.
Pannaccione, A., Piccialli, I., Secondo, A., Ciccone, R., Molinaro, P., Boscia, F., Annunziato, L., 2020. The Na(+)/Ca(2+)exchanger in Alzheimer's disease. Cell Calcium 87, 102190. https://doi.org/10.1016/j.ceca.2020.102190.
Pannaccione, A., Secondo, A., Molinaro, P., D'Avanzo, C., Cantile, M., Esposito, A., Annunziato, L., 2012. A new concept: Abeta1-42 generates a hyperfunctional proteolytic NCX3 fragment that delays caspase-12 activation and neuronal death. J. Neurosci. 32 (31), 10609–10617. https://doi.org/10.1523/JNEUROSCI.6429-11.2012.
Papa, M., Canitano, A., Boscia, F., Castaldo, P., Sellitti, S., Porzig, H., Annunziato, L., 2003. Differential expression of the Na+-Ca2+ exchanger transcripts and proteins in rat brain regions. J. Comp. Neurol. 461 (1), 31–48. https://doi.org/10.1002/cne.10665.
Pappalardo, L.W., Samad, O.A., Black, J.A., Waxman, S.G., 2014. Voltage-gated sodium channel Nav 1.5 contributes to astrogliosis in an in vitro model of glial injury via reverse Na+ /Ca2+ exchange. Glia 62 (7), 1162–1175. https://doi.org/10.1002/glia.22671.
Pasinelli, P., Brown, R.H., 2006. Molecular biology of amyotrophic lateral sclerosis: insights from genetics. Nat. Rev. Neurosci. 7 (9), 710–723. https://doi.org/10.1038/nrn1971.
Philips, T., Rothstein, J.D., 2014. Glial cells in amyotrophic lateral sclerosis. Exp. Neurol. (262 Pt B), 111–120. https://doi.org/10.1016/j.expneurol.2014.05.015.
Pignataro, G., Gala, R., Cuomo, O., Tortiglione, A., Giaccio, L., Castaldo, P., Annunziato, L., 2004. Two sodium/calcium exchanger gene products, NCX1 and NCX3, play a major role in the development of permanent focal cerebral ischemia. Stroke 35 (11), 2566–2570. https://doi.org/10.1161/01.str.0000143730.29964.93.
Pignataro, G., Sirabella, R., Anzilotti, S., Di Renzo, G., Annunziato, L., 2014. Does Na(+)/Ca(2)(+) exchanger, NCX, represent a new druggable target in stroke intervention? Transl. Stroke Res. 5 (1), 145–155. https://doi.org/10.1007/s12975-013-0308-8.
Pignataro, G., Ziaco, B., Tortiglione, A., Gala, R., Cuomo, O., Vinciguerra, A., Cataldi, M., 2015. Neuroprotective effect of VEGF-mimetic peptide QK in experimental brain ischemia induced in rat by middle cerebral artery occlusion. ACS Chem. Neurosci. 6 (9), 1517–1525. https://doi.org/10.1021/acschemneuro.5b00175.
Quednau, B.D., Nicoll, D.A., Philipson, K.D., 1997. Tissue specificity and alternative splicing of the Na+/Ca2+ exchanger isoforms NCX1, NCX2, and NCX3 in rat. Am. J. Phys. 272 (4 Pt 1), C1250–C1261. https://doi.org/10.1152/ajpcell.1997.272.4.C1250.
Rosen, D.R., Siddique, T., Patterson, D., Figlewicz, D.A., Sapp, P., Hentati, A., 1993. Mutations in Cu/Zn superoxide dismutase gene are associated with familial amyotrophic lateral sclerosis. Nature 362 (6415), 59–62. https://doi.org/10.1038/362059a0.
Secondo, A., Pignataro, G., Ambrosino, P., Pannaccione, A., Molinaro, P., Boscia, F., Annunziato, L., 2015. Pharmacological characterization of the newly synthesized 5-amino-N-butyl-2-(4-ethoxyphenoxy)-benzamide hydrochloride (BED) as a potent NCX3 inhibitor that worsens anoxic injury in cortical neurons, organotypic hippocampal cultures, and ischemic brain. ACS Chem. Neurosci. 6 (8), 1361–1370. https://doi.org/10.1021/acschemneuro.5b00043.
Severino, B., Corvino, A., Fiorino, F., Frecentese, F., Perissutti, E., Caliendo, G., De Nucci, G., 2019. Development, validation of LC-MS/MS method and determination

of pharmacokinetic parameters of the stroke neuroprotectant neurounina-1 in beagle dog plasma after intravenous administration. Front. Pharmacol. 10, 432. https://doi.org/10.3389/fphar.2019.00432.

Siklos, L., Engelhardt, J., Harati, Y., Smith, R.G., Joo, F., Appel, S.H., 1996. Ultrastructural evidence for altered calcium in motor nerve terminals in amyotropic lateral sclerosis. Ann. Neurol. 39 (2), 203–216. https://doi.org/10.1002/ana.410390210.

Siklos, L., Engelhardt, J.I., Alexianu, M.E., Gurney, M.E., Siddique, T., Appel, S.H., 1998. Intracellular calcium parallels motoneuron degeneration in SOD-1 mutant mice. J. Neuropathol. Exp. Neurol. 57 (6), 571–587. https://doi.org/10.1097/00005072-199806000-00005.

Sokolow, S., Luu, S.H., Headley, A.J., Hanson, A.Y., Kim, T., Miller, C.A., Gylys, K.H., 2011. High levels of synaptosomal Na(+)-Ca(2+) exchangers (NCX1, NCX2, NCX3) co-localized with amyloid-beta in human cerebral cortex affected by Alzheimer's disease. Cell Calcium 49 (4), 208–216. https://doi.org/10.1016/j.ceca.2010.12.008.

Tateno, M., Sadakata, H., Tanaka, M., Itohara, S., Shin, R.M., Miura, M., Takahashi, R., 2004. Calcium-permeable AMPA receptors promote misfolding of mutant SOD1 protein and development of amyotrophic lateral sclerosis in a transgenic mouse model. Hum. Mol. Genet. 13 (19), 2183–2196. https://doi.org/10.1093/hmg/ddh246.

Valsecchi, V., Anzilotti, S., Serani, A., Laudati, G., Brancaccio, P., Guida, N., Annunziato, L., 2020a. miR-206 reduces the severity of motor neuron degeneration in the facial nuclei of the brainstem in a mouse model of SMA. Mol. Ther. https://doi.org/10.1016/j.ymthe.2020.01.013.

Valsecchi, V., Boido, M., De Amicis, E., Piras, A., Vercelli, A., 2015. Expression of muscle-specific MiRNA 206 in the progression of disease in a murine SMA model. PLoS One 10 (6), e0128560. https://doi.org/10.1371/journal.pone.0128560.

Van Damme, P., Dewil, M., Robberecht, W., Van Den Bosch, L., 2005. Excitotoxicity and amyotrophic lateral sclerosis. Neurodegener. Dis. 2 (3–4), 147–159. https://doi.org/10.1159/000089620.